NATIONAL ADVISORY COMMITTEE FOR AERONAUTICS

WARTIME REPORT

ORIGINALLY ISSUED
October 1944 as
Advance Restricted Report L4H15

FULL-SCALE WIND-TUNNEL INVESTIGATION OF FORWARD UNDERSLUNG COOLING-AIR DUCTS

By W. J. Nelson, K. R. Czarnecki,
and Robert D. Harrington

Langley Memorial Aeronautical Laboratory
Langley Field, Va.

NACA

WASHINGTON

NACA ARR No. L4H15

NATIONAL ADVISORY COMMITTEE FOR AERONAUTICS

ADVANCE RESTRICTED REPORT

FULL-SCALE WIND-TUNNEL INVESTIGATION OF FORWARD UNDERSLUNG COOLING-AIR DUCTS

By W. J. Nelson, K. R. Czarnecki
and Robert D. Harrington

SUMMARY

A general investigation of underslung cooling-air ducts in various locations on a model of a typical single-engine tractor airplane has been conducted in the NACA full-scale tunnel. This report contains the results of tests of two forward underslung ducts. These tests were made to determine the effect of the inlet-velocity ratio, the angle of attack, the radiator resistance, and the propeller operation on the pressure recovery at the radiator, on the drag of the cooling installation, and on the critical speed of the ducts. Pressure measurements were made at the duct inlets and at the face of the radiator to determine the diffuser losses, and at the duct outlets to find the volume rate of air flow through the duct. The drag of the various duct installations was obtained from force tests of the model with the ducts installed and removed. Static-pressure distributions were taken at the duct lips and at the duct-fuselage fillets to determine the critical speed of the ducts.

At low values of lift coefficient, with the propeller removed, pressure recoveries greater than 90 percent of the free-stream dynamic pressure were obtained at values of inlet-velocity ratio from 0.40 to 0.75. Propeller operation increased the pressure recovery 7 percent of the free-stream dynamic pressure at a thrust coefficient of 0.02 and about 45 percent of the free-stream dynamic pressure at a thrust coefficient of 0.11. Reductions in the outlet static pressure as large as 50 percent of the free-stream dynamic pressure were obtained by the installation of 45° exit flaps with the propeller removed, and even greater reductions were noted with the propeller operating. The lowest critical speed was measured at the left duct-fuselage fillet with the propeller operating.

INTRODUCTION

A general investigation of charge-air and cooling-air ducts, installed in a full-scale model of the Republic XP-47 airplane, has been made in the NACA full-scale tunnel to provide a basis for comparing several typical duct installations with regard to the pressure recoveries obtainable at the radiators, the drag of the complete ducting system, and the critical speed of the inlet lips. The results of tests of the engine-charge-air ducts with inlets located on the top of the fuselage and of the cooling-air ducts with inlets located in the wings and on the bottom of the fuselage behind the leading edge of the wing are given in references 1 to 3. The results of the tests of the underslung ducts with inlets close to the propeller are presented in this report.

Tests were made to determine the performance of a large and a small forward underslung duct over a range of airplane angles of attack, duct inlet-velocity ratios, and radiator resistances. Most of the tests were made with the propeller removed from the airplane. Some tests were made, however, with the propeller operating to determine the effects of the slipstream on the duct characteristics.

SYMBOLS

C_L	lift coefficient
T_c	thrust coefficient $\left(\frac{T}{\rho V_o^2 D^2}\right)$
ΔC_D	increment of drag coefficient due to duct
ΔC_{D_i}	calculated increment of internal-drag coefficient
ΔC_{D_e}	increment of drag coefficient due to external drag of duct $\left(\Delta C_D - \Delta C_{D_i}\right)$
ΔD	increment of drag due to duct
T	thrust
ρ	mass density of air

V	velocity
D	propeller diameter
A	cross-sectional area of duct
S	wing area
p	local static pressure
q	dynamic pressure
Δp	pressure drop across orifice plate representing radiator
$\frac{\Delta p}{q_2}$	pressure-drop coefficient for orifice plate
H	total pressure
Q	volume rate of flow
Q/V_o	air-flow parameter
V_1/V_o	inlet-velocity ratio
η	duct efficiency ($Q\ \Delta p/\Delta DV_o$)
α	angle of attack of thrust axis relative to free-stream direction
β	propeller blade angle at 0.75 radius

Subscripts (denoting average conditions):

o	in free stream
1	in duct inlet
2	at front face of orifice plate
3	at duct outlet
cr	critical

APPARATUS AND METHODS

The model used in these tests is a typical low-wing single-engine fighter airplane with a wing area of 170 square feet. The general arrangement of the model and the basic dimensions are given in figure 1. For the tests with the propeller operating, the model was equipped with a 10-foot-diameter Curtiss controllable-pitch propeller that was driven by an electric motor. The propeller had 6146cl.5-24 blades, the shanks of which were covered with cuffs shown in figure 2. The model is shown mounted in the NACA full-scale tunnel in figure 3. A description of the NACA full-scale tunnel and the balance equipment used in these tests is given in reference 4.

The large and small forward underslung ducts are shown installed on the model in figures 4 and 5, respectively. Photographs of the inlets and outlets are shown in figures 6 and 7 and the general dimensions of the ducts are given in figures 8 and 9. Each duct was tested with three outlets in order to vary the volume rate of air flow. These figures show that the outlet area of the ducts was varied by cutting back the duct exit from the original position. Some additional tests were made to determine the effect on the pressure distribution and total-pressure recovery at the face of the radiator of three equally spaced radial vanes installed in the diffuser of the large duct.

Total-pressure measurements were made at the duct inlet and at the front of the radiator to determine the pressure loss in the diffuser. The volume rate of flow through each duct was calculated from measurements of total and static pressures in the duct outlets. Static-pressure distributions, for the purpose of estimating the critical speeds of the duct lips and the duct-fuselage fillets, were determined by use of rows of $\frac{1}{32}$-inch static-pressure orifices mounted flush with the outer surface of the section. The ordinates of the lower lips are given in table I.

The effect of the slipstream on the duct performance was obtained with the propeller operating at thrust coefficients simulating the sea-level high-speed and

climbing-flight conditions for an airplane with a normal rating of 1600 horsepower. For the high-speed condition, $C_L = 0.10$, the propeller blade angle was 60° and the thrust coefficient was 0.02. For the climb condition, $C_L = 0.47$, the blade angle was 40° and the thrust coefficient 0.11.

The effect of the various duct installations on the drag of the model was determined from the force tests with the duct installed on the airplane and with the duct removed. These force tests were made over a range of lift coefficient from -0.2 to 0.5 at a tunnel air velocity of approximately 96 miles per hour. The increments of internal drag were calculated from the volume rate of air flow and the exit total pressure.

The relationship between the lift coefficient and the angle of attack for this airplane is given in figure 10.

RESULTS AND DISCUSSION

The presentation of the results is divided into four sections in which the requirements for satisfactory duct performance are discussed. These requirements include (1) high pressure recovery at the front of the radiator, (2) low available outlet static pressures for adequate control of flow through the radiator, (3) low drag over the speed range from high speed to climbing speed, and (4) high critical speed of the duct. In the first section the effects of the inlet-velocity ratio, the lift coefficient, and the propeller thrust on the pressure recovery at the radiator are discussed. In the second section the static pressure at the duct outlet is discussed as a function of the geometric dimensions of the outlet section of the duct, the lift coefficient, and the thrust coefficient. In the same section the effect on the outlet static pressure of installing outlet flaps is described. The internal drag caused by flow through the duct and the external drag caused by flow disturbances over the duct are discussed separately in the third section. The effects of the inlet-velocity ratio, the lift coefficient, and the propeller operation on the critical speed of the ducts are discussed in the fourth section.

Pressure Recoveries at Radiator

The total-pressure recovery at the radiator is determined by the losses that occur at the duct inlet and in the duct diffuser. The pressure losses at the inlet are caused by separation of the boundary layer from the fuselage surface just ahead of the inlet. Since the boundary layer at the inlet to a forward underslung duct is usually very thin, there is little tendency toward separation and the inlet losses are very small (fig. 11) over the normal range of design inlet-velocity ratio V_1/V_o from 0.4 to 1.0. It is therefore apparent that total-pressure recoveries appreciably below the full free-stream dynamic pressure will occur in forward underslung ducts only when there are large pressure losses in the diffuser. The losses that occur in the diffuser are discussed in the following paragraphs as a function of the inlet-velocity ratio, the lift coefficient, and the propeller thrust.

Effect of inlet-velocity ratio.- The variation of the average total pressure at the face of the orifice plate with the inlet-velocity ratio is shown in figure 12. At a lift coefficient of 0.10, with the propeller removed, pressure recoveries greater than 90 percent of the free-stream dynamic pressure ($0.90q_o$) were recorded in both the large and the small forward underslung ducts at values of V_1/V_o from 0.40 to 0.75. The inlet-velocity ratio at which the peak recovery was obtained and the range of inlet-velocity ratios over which high pressure recoveries were obtained decreased with increasing lift coefficients. From the scatter of the test points, it is evident that any differences in recovery caused by changes in the resistance of the radiator are well within the accuracy of the measurements.

The pressures at the face of the orifice plate are presented as contour maps in figure 13. At $C_L = 0.10$ and $V_1/V_o = 0.53$ the total-pressure recovery was high and uniform over the central part of the radiator and decreased slowly toward the edges. Increasing the inlet-velocity ratio to 0.74 reduced the recovery near the duct walls still further. At $V_1/V_o = 0.94$ very low pressures were measured at the bottom of the radiator, which indicated that separation occurred in the lower part of the diffuser.

For corresponding inlet-velocity ratios, the pressure losses at $C_L = 0.89$ were greater than the pressure losses at $C_L = 0.10$.

The effect of changing the inlet-velocity ratio on the flow over a duct lip is analogous to changing the angle of attack of an airfoil. At low values of V_1/V_o, the streamlines expand ahead of the duct and in effect cause the duct lip to operate as an airfoil at a high angle of attack (sketch (a)), with the inner

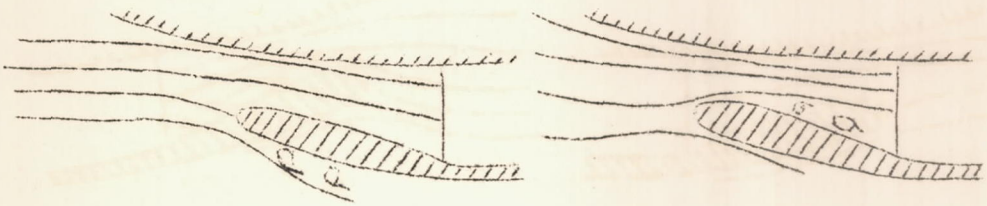

(a) $V_1/V_o < 0.4$. (b) $V_1/V_o \cong 1.0$.

surface of the lip corresponding to the lower surface of the airfoil. In this condition the flow over the inner surface of the lip is smooth, but on the outer surface there is a tendency toward high negative pressures and separation from the lip. With increasing inlet-velocity ratios, the angle of attack of the lip decreases until at some inlet velocity the lip operates at a negative angle of attack (sketch (b)) and the tendency toward separation occurs on the inner surface of the lip. The exact value of V_1/V_o at which separation, if any, will occur depends upon the camber, the leading-edge radius, and the alinement of the duct lip.

Effect of lift coefficient.- In order to determine the effect of changes of lift coefficient on the pressure at the face of the orifice plate, tests were made with constant outlet area and flap position at lift coefficients ranging from 0.1 to 0.9. The results of these tests (figs. 14 and 15) show that increasing C_L decreased both the recovery and the inlet-velocity ratio. In order to separate the changes in recovery caused by varying the lift coefficient from those associated with the variations in inlet-velocity ratio, the curves of figure 12 have been cross-plotted at constant values of V_1/V_o and are presented in figure 16. These data show that, over a range of lift coefficient from 0.1 to 0.9, the total-pressure recovery at inlet-velocity ratios of about 0.5 varied less than $0.05q_o$ and that

the adverse effect of changes in C_L increased rapidly with inlet-velocity ratio.

The effects of lift coefficient on the pressure recovery at the radiator are readily explained by the airfoil analogy used in the preceding section. At low lift coefficients the duct lip is alined with the approaching air stream and the flow over the lip is smooth (sketch (c)). As C_L increases, the stagnation

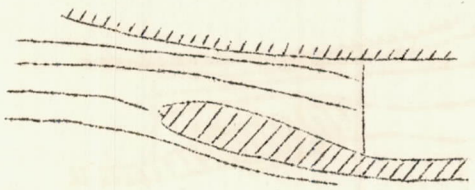

(c) Low C_L.

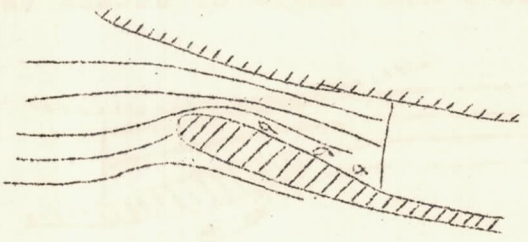

(d) High C_L.

point moves to the under side of the lip and the flow tends to separate from the lower wall of the duct (sketch (d)).

With vanes installed in the diffuser the recovery at $C_L = 0.10$ was slightly lower than without vanes (fig. 14); the vanes, however, reduced the adverse effects of increasing lift coefficient.

Propeller operation.- The effect of the propeller operation on the variation of the total pressure at the face of the orifice plate with inlet-velocity ratio is shown in figure 17 for the large forward underslung duct. In the high-speed attitude, $C_L = 0.10$ and $V_1/V_o = 0.5$, the pressure recovery with the propeller operating at $T_c = 0.02$ was about $0.07q_o$ greater than that with the propeller removed. In the climb condition, $C_L = 0.47$, $T_c = 0.11$, and $V_1/V_o = 0.8$, the total pressure at the radiator was $0.45q_o$ greater than with the propeller removed. These data show that the range of inlet-velocity ratios over which the pressure recovery remains substantially constant was much greater with the propeller operating than with the propeller removed. For convenience in comparison, the inlet-velocity ratio with the propeller operating has been based on the free-stream velocity and not on the velocity in the slipstream.

The substantial increase in the total pressure obtained at the face of the radiator with the propeller operating, particularly at the climb thrust coefficient, is largely attributed to the cuffs installed on the shanks of the propeller blades. Ordinarily, this portion of the propeller, with its poor blade sections, contributes little to the propeller thrust. With the cuffs installed, however, a more nearly uniform radial propeller-load distribution is possible with a resultant increase in the total pressure behind the inner sections of the propeller blade. This effect becomes greater for the high propeller loadings of the climb condition. The cuffs also serve to increase the critical speed of the propeller-blade shanks.

Results obtained with constant outlet area show the effect of the propeller operation on both the pressure recovery and the inlet-velocity ratio. (See fig. 18.) At the high-speed T_c of 0.02, a slight increase in the pressure recovery and the inlet-velocity ratio was caused by propeller operation; at the climb T_c of 0.11, however, the increases in the recovery and in the inlet-velocity ratio were much larger.

Typical pressure distributions at the radiator with the propeller removed and operating are presented in figure 19. In the high-speed attitude, $C_L = 0.10$, at an inlet-velocity ratio of 0.58, the slipstream at $T_c = 0.02$ increased the total pressure at the radiator approximately $0.07q_o$ with no great change in the distribution. In the climb attitude, $C_L = 0.47$, with the propeller operating at $T_c = 0.11$, the average total pressure at the radiator was $0.40q_o$ greater than for the propeller-removed tests. The contour map indicates that the core of high pressures which was concentrated in the upper part of the radiator in the propeller-removed tests has moved to the center of the duct.

The effects of propeller operation with the small forward underslung duct are given in table II. These data are insufficient to make as thorough an analysis as for the large duct, but the effects appear to be generally similar. In the climb attitude with $T_c = 0.11$, the average total pressure at the radiator was lower, at low values of V_1/V_o, for the small duct than for the large duct. (See table II and fig. 17.) It is probable

that at the low values of V_1/V_o a greater proportion of the air entering the small duct inlet is affected by the less efficient inner portion of the propeller blade.

Pressures behind Radiator

The quantity of air flowing through a duct may be determined from the total- and static-pressure measurements at the duct exit. The static pressure at the duct exit is primarily dependent upon the convergence of the outlet section of the duct and the angle at which the flow from the duct is discharged into the free stream. When the air is discharged from a rapidly contracting outlet section, its velocity continues to increase for some distance downstream of the exit and usually results in static pressures at the outlet that are higher than the pressure of the neighboring free stream.

Discharging the air at too great an angle to the free stream changes the adjacent external static pressure, and consequently the exit static pressure, as a result of an effective thickening of the body in the region just behind the exit. Some of these effects and the effects of changes in angle of attack of the model and propeller operation on the outlet static pressures are discussed in the following paragraphs.

Effect of outlet design.- Shortening the outer skirt of the outlet fairing to increase the outlet size also changed the rate of convergence and angle of discharge of the outlet. (See figs. 8 and 9.) The effect of these changes on the static pressure in the outlet is shown in figures 20 and 21. These plots indicate that the lowest static pressures will occur in slowly converging outlets discharging the cooling-air flow parallel to the local external stream. The static pressure in the outlet will be identical with the static pressure of the outside flow at the opening if the outlet duct is so designed that the streamline dividing the internal and external fields is straight.

Effect of exit flaps.- The effect of installing exit flaps was to decrease the exit static pressure by approximately $0.55q_o$ in the exits of both the large and small ducts. Average static pressures as low as $-0.45q_o$ were obtained with the propeller removed, values which are indicative of good exit-flap effectiveness.

Effect of lift coefficient.- The variation of average outlet static pressure with lift coefficient is shown in figures 22 and 23. Increasing the lift coefficient of the airplane increased the static pressure at the duct outlets. The increase was approximately $0.15q_o$ without exit flaps and approximately twice that value with 45° exit flaps installed, when the lift coefficient was increased from 0.10 to 0.89. The effect is attributed to a rearward movement of the stagnation region on the bottom of the fuselage when the angle of attack of the airplane is increased.

Effect of propeller operation.- The effect of propeller operation on the outlet static pressure may be obtained by a comparison of figures 20 and 24. At $C_L = 0.10$ and with no exit flap, the difference between the propeller-operating ($T_c = 0.02$) and the propeller-removed static pressures was negligible. At $T_c = 0.11$, for which case $C_L = 0.47$, the static pressure increased slightly with no outlet flaps and decreased from $-0.09q_o$ to $-0.23q_o$ with outlet flaps installed. With an average total pressure of about $1.20q_o$ at the face of the radiator (fig. 17) and an average outlet static pressure of $-0.40q_o$ (fig. 24), a pressure difference of approximately $1.60q_o$ is available for forcing air through the duct in the climb attitude with the propeller operating at $T_c = 0.11$.

Drag and Duct Efficiency

A summary of the drag data for the model with the large and small forward underslung ducts installed is presented in tables III and IV. The increment of the drag coefficient due to the duct ΔC_D is the difference between the drag of the model with the duct installed and with the duct removed.

In order to facilitate analysis, the drag increment is divided into two parts: (1) the drag caused by losses in the duct (internal drag) and (2) the drag caused by changes in the external flow (external drag). The increment of internal drag coefficient is equal to the momentum loss through the duct calculated by the formula

$$\Delta C_{D_i} = \frac{2Q}{SV_o}\left(1 - \sqrt{\frac{H_3 - p_o}{q_o}}\right)$$

The external drag is the difference between the calculated ΔC_{D_i} and the total increment measured by the force tests and may be expressed as

$$\Delta C_{D_e} = \Delta C_D - \Delta C_{D_i}$$

The increase in drag that accompanied the increase in the outlet area of the ducts was due mainly to an increase in the internal drag of the installations as a result of the larger volume rate of air flow. The larger volume rate of flow caused an increase in the pressure drop across the orifice plate and generally increased the diffuser pressure losses. The increment of total drag coefficient ΔC_D due to the large forward underslung duct varied from 0.0011 to 0.0029 and for the small duct from 0.0013 to 0.0022 (tables III and IV), depending upon the nominal pressure drop of the radiator and the volume rate of air flow.

In order to compare the internal drag of the two ducts, the internal-drag coefficient has been plotted as a function of the inlet-velocity ratio in figure 25. This figure shows that, for equal values of pressure drop for the orifice plate and inlet-velocity ratio, the internal-drag coefficient of the small duct was higher in some instances than that of the large duct. The internal-drag coefficient was higher even though at equal values of V_1/V_o the volume rate of air flow through the smaller duct was less than that for the large duct. The higher internal drag of the small duct is caused by the difference in the expansion between the inlet and the radiator. The ratio of orifice-plate area to inlet area is 2.5 for the large duct and 2.0 for the small duct (see figs. 8 and 9); thus, for a given V_1/V_o and $\Delta p/q_2$ the dynamic pressure q_2 and hence the pressure drop Δp and the over-all pressure drop $H_o - H_3$ in the small duct are greater than in the large duct.

The calculated increment of drag coefficient due to the external drag of the duct ΔC_{D_e} varied from 0 to 0.0010 with the large duct installed and from 0 to 0.0004 with the small duct installed. (See tables III and IV.) In the case of the small duct, the increment of external drag generally increased with $\Delta p/q_2$ and appeared to be approximately the same for both the

medium and the large outlets. With the large duct installed, the values of ΔC_{D_e} increased with the size of the outlet and appeared to decrease with increasing $\Delta p/q_2$. A major part of the increment of external drag is attributed to the interference effects associated with the mixing of two streams of unequal velocity and with different flow directions.

The efficiency of each duct η, defined as the ratio of the minimum power required to force the cooling air through the radiator to the power needed to overcome the drag of the complete installation, has been calculated and the values are presented in tables III and IV. At inlet-velocity ratios below 0.62 the efficiency of the large duct was greater than 70 percent but decreased rapidly above an inlet-velocity ratio of about 0.70. The efficiency of the small duct was consistently lower than that of the large duct at the same V_1/V_0 and $\Delta p/q_2$ values because of the relatively higher internal drag.

Critical Speeds

The critical speeds of the duct inlet lips were estimated from the surface static pressures measured at a tunnel speed of 96 miles per hour by using the von Kármán-Tsien pressure extrapolation obtained from reference 5. These extrapolations are shown in figure 26. The minimum pressure coefficients $\frac{p - p_o}{q_o}$ were determined from pressure distributions measured over the lip at the bottom of the duct inlet and in the duct-fuselage fillets.

Effect of inlet-velocity ratio.- The critical Mach number increased linearly with the inlet-velocity ratio as shown in figure 27 for the small duct. Typical pressure distributions over the lip of the small forward underslung duct (fig. 28) show the change in distribution that accompanied changes in inlet-velocity ratio. It is noted that the stagnation point moves outward as V_1/V_0 increases and that the peak negative pressures are reduced.

Effect of lift coefficient.- In figure 29 the critical Mach number of the small forward underslung duct is shown as a function of the lift coefficient of

the airplane with propeller removed. Increasing the lift coefficient caused substantial increases in the critical speed of the lower part of the duct lip but decreased the critical speed of the sections along the duct-fuselage fillets. The rate of change of critical Mach number with lift coefficient was much greater at the bottom of the ducts than in the fillets.

Effect of propeller operation.- The critical Mach number of the various sections of the lip of the small duct, determined from tests with the propeller removed and with the propeller operating, are shown as a function of the inlet-velocity ratio in figure 30. At the bottom of the duct lip, the critical speed of the section varied slightly and irregularly with propeller operation. Along the left fillet, M_{cr} was slightly lower with propeller operating; whereas, along the right fillet the critical speed was substantially greater with propeller operating than with the propeller removed. This effect is probably due to the slipstream rotation which decreases the effective angle of attack on the right side of the duct behind the downgoing propeller blades and increases the effective angle of attack on the left side of the duct behind the upgoing propeller blades.

The critical speed of the left fillet for the high-speed condition, $C_L = 0.10$, $T_c = 0.02$, and $V_1/V_o = 0.50$, was estimated to be about 485 miles per hour at standard sea-level conditions. The critical speed of both the lower duct lip and the right duct-fuselage fillet were higher than the critical speed of the left fillet.

A similar but less thorough investigation was made of the critical speed of the inlet to the large duct with similar results which are not presented here.

SUMMARY OF RESULTS

Tests of forward underslung ducts on a typical fighter airplane in the NACA full-scale tunnel, indicated that:

1. Pressure recoveries at the radiator greater than 90 percent of the free-stream dynamic pressure

were obtainable at the low lift coefficient of 0.10, with the propeller removed, for inlet-velocity ratios ranging from 0.40 to 0.75. Beyond the inlet-velocity ratio of 0.75 the pressure recoveries decreased rapidly.

2. The variation of pressure recovery with lift coefficient, with the propeller removed, was less than 5 percent of the free-stream dynamic pressure at values of inlet-velocity ratio of 0.5; for inlet-velocity ratios greater than 0.5 the pressure losses ahead of the radiator increased rapidly with lift coefficient.

3. Vanes in the diffuser of the forward underslung duct had little effect on the pressure recovery at low lift coefficients but reduced the adverse effects of increasing lift coefficient.

4. Operation of the propeller, equipped with large-chord cuffs, increased the total pressure at the radiator of the large duct approximately 7 percent of the free-stream dynamic pressure at the high-speed thrust coefficient of 0.02 and approximately 45 percent of the free-stream dynamic pressure at the climb thrust coefficient of 0.11.

5. The static pressure at the outlet with no exit flaps was positive and with and without exit flaps increased with both the lift coefficient and the propeller thrust.

6. With the propeller removed, the static pressure at the outlet was reduced approximately 50 percent of the free-stream dynamic pressure by installing 45° exit flaps; the effectiveness of the exit flaps increased considerably with power.

7. At equal values of inlet-velocity ratio and pressure-drop coefficient for the orifice plate, the internal drag of the small duct was somewhat higher in some instances than that of the larger duct even though the air flow was considerably less. The higher drag was a result of the lower diffuser expansion ratio of the small duct, which resulted in a higher dynamic pressure within the duct and hence greater pressure losses and a greater pressure drop across the radiator. No comparison was made of the ducts on the basis of providing equal cooling.

8. Increases in the inlet-velocity ratio with the propeller removed increased the critical Mach number of the duct lower lip and duct-fuselage fillets.

9. Increases in the lift coefficient of the airplane with propeller removed increased the critical speed of the duct lip but decreased the critical speed of the fillets.

10. Propeller operation had little effect on the critical speed of the lower lip. The critical speed of the left fillet was only slightly decreased by propeller operation; whereas, a substantial increase was measured at the right fillet.

Langley Memorial Aeronautical Laboratory
National Advisory Committee for Aeronautics
Langley Field, Va.

REFERENCES

1. Nelson, W. J., and Czarnecki, K. R.: Wind-Tunnel Investigation of Carburetor-Air Inlets. NACA ARR, Feb. 1942.

2. Nelson, W. J., and Czarnecki, K. R.: Wind-Tunnel Investigation of Wing Ducts on a Single-Engine Pursuit Airplane. NACA ARR No. 3J13, 1943.

3. Czarnecki, K. R., and Nelson, W. J.: Wind-Tunnel Investigation of Rear Underslung Fuselage Ducts. NACA ARR No. 3I21, 1943.

4. DeFrance, Smith J.: The N.A.C.A. Full-Scale Wind Tunnel. NACA Rep. No. 459, 1933.

5. von Kármán, Th.: Compressibility Effects in Aerodynamics. Jour. Aero. Sci., vol. 8, no. 9, July 1941, pp. 337-356.

TABLE I

ORDINATES OF LOWER LIPS OF LARGE AND SMALL FORWARD UNDERSLUNG DUCTS

[All values are in inches]

x	Large duct		Small duct	
	y_U	y_L	y_U	y_L
0	0.5	-0.83	0.45	-0.7
.25	.47	-1.0	.35	-.95
.50	.40	-1.17	.28	-1.10
.75	.31	-1.35	.20	-1.30
1.0	.19	-1.48	.10	-1.45
1.25	.08	-1.63	0	-1.62
1.5	-.03	-1.75	-.08	-1.75
1.75	-.10	-1.85	-.20	-1.90
2.0	-.18	-1.95	-.27	-2.0
2.5	-.33	-2.13	-.45	-2.22
3.0	-.50	-2.30	-.61	-2.39
3.5	-.63	-2.45	-.78	-2.5
4.0	-.78	-2.63	-.95	-2.63
4.5	-.93	-2.80	-1.10	-2.75
5.0	-1.05	-2.95	-1.29	-2.88
6.0	-1.30	-3.27	-1.60	-3.10
7.0	-1.60	-3.58	-1.89	-3.31
8.0	-1.90	-3.85	-2.10	-3.47

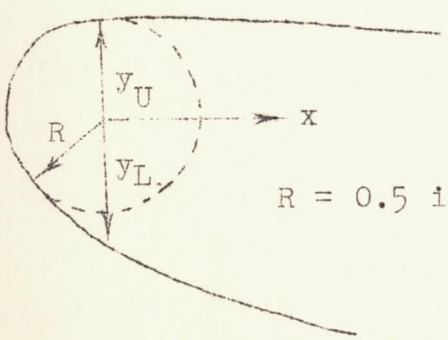

R = 0.5 in.

Large duct

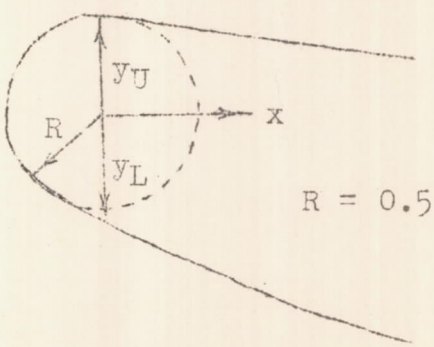

R = 0.5 in.

Small duct

TABLE II

COMPARISON OF PROPELLER-REMOVED AND PROPELLER-OPERATING DATA

FOR SMALL FORWARD UNDERSLUNG DUCT

C_L	Nominal $\Delta p/q_2$	Outlet	Exit flap	$(H_2 - p_o)/q_o$		V_1/V_o		Q/V_o		$(p_3 - p_o)/q_o$	
				Propeller		Propeller		Propeller		Propeller	
				Removed	Operating	Removed	Operating	Removed	Operating	Removed	Operating
0.10	10.1	Small	Off	0.96	1.02	0.40	0.43	0.31	0.33	0.14	0.14
.10	10.1	Medium	Off	.95	-----	.44	.46	.34	.36	.11	.09
.10	6.0	Small	Off	.93	1.02	.48	.61	.37	.47	.18	.19
.10	6.0	Medium	Off	.95	1.01	.54	.54	.42	.42	.13	.18
.10	1.7	Small	Off	.97	1.02	.58	.66	.45	.48	.21	.19
.10	1.7	Medium	Off	.94	.99	.64	.70	.50	.54	.17	.18
.47	10.1	Medium	On	.90	1.03	.52	.63	.40	.48	-.29	-.49
.47	6.0	Medium	On	.90	1.12	.65	.78	.50	.60	-.31	-.59
.47	1.7	Medium	On	.79	1.20	.82	.98	.63	.78	-.34	-.59

Power condition	C_L	β (deg)	T_c
High speed	0.10	60	0.02
Climb	.47	40	.11

NATIONAL ADVISORY
COMMITTEE FOR AERONAUTICS

TABLE III

SUMMARY OF DRAG DATA FOR LARGE

FORWARD UNDERSLUNG DUCT

[C_L = 0.10; exit flaps off]

Outlet	Nominal $\Delta p/q_2$	Q/V_o	V_1/V_o	ΔC_D at C_L = 0.10			η
				ΔC_D	ΔC_{D_i}	ΔC_{D_e}	
Small[a]	11.2	0.52	0.50	------	0.0017	------	----
Medium	11.2	.59	.57	0.0028	.0026	0.0002	0.76
Large	11.2	.54	.52	------	.0025	------	----
Small	3.3	.64	.62	.0011	.0011	.0000	.73
Small[a]	3.3	.62	.60	------	.0009	------	----
Medium	3.3	.76	.74	.0020	.0016	.0004	.64
Large	3.3	.76	.74	.0029	.0019	.0010	.46

[a]Vanes installed in diffuser.

TABLE IV

SUMMARY OF DRAG DATA FOR SMALL

FORWARD UNDERSLUNG DUCT

[C_L = 0.10; exit flaps off]

Outlet	Nominal $\Delta p/q_2$	Q/V_o	V_1/V_o	ΔC_D at C_L = 0.10			η
				ΔC_D	ΔC_{D_i}	ΔC_{D_e}	
Small	10.1	0.31	0.40	------	0.0013	------	----
Medium	10.1	.34	.44	0.0018	.0018	0.0000	0.52
Large	10.1	.34	.44	.0021	.0017	.0004	.45
Small	6.0	.37	.48	------	.0011	------	----
Medium	6.0	.42	.55	.0018	.0016	.0002	.58
Large	6.0	.42	.55	.0022	.0020	.0002	.49
Small	1.7	.45	.58	------	.0007	------	----
Medium	1.7	.50	.65	.0013	.0012	.0001	.38
Large	1.7	.50	.65	.0017	.0016	.0001	.41

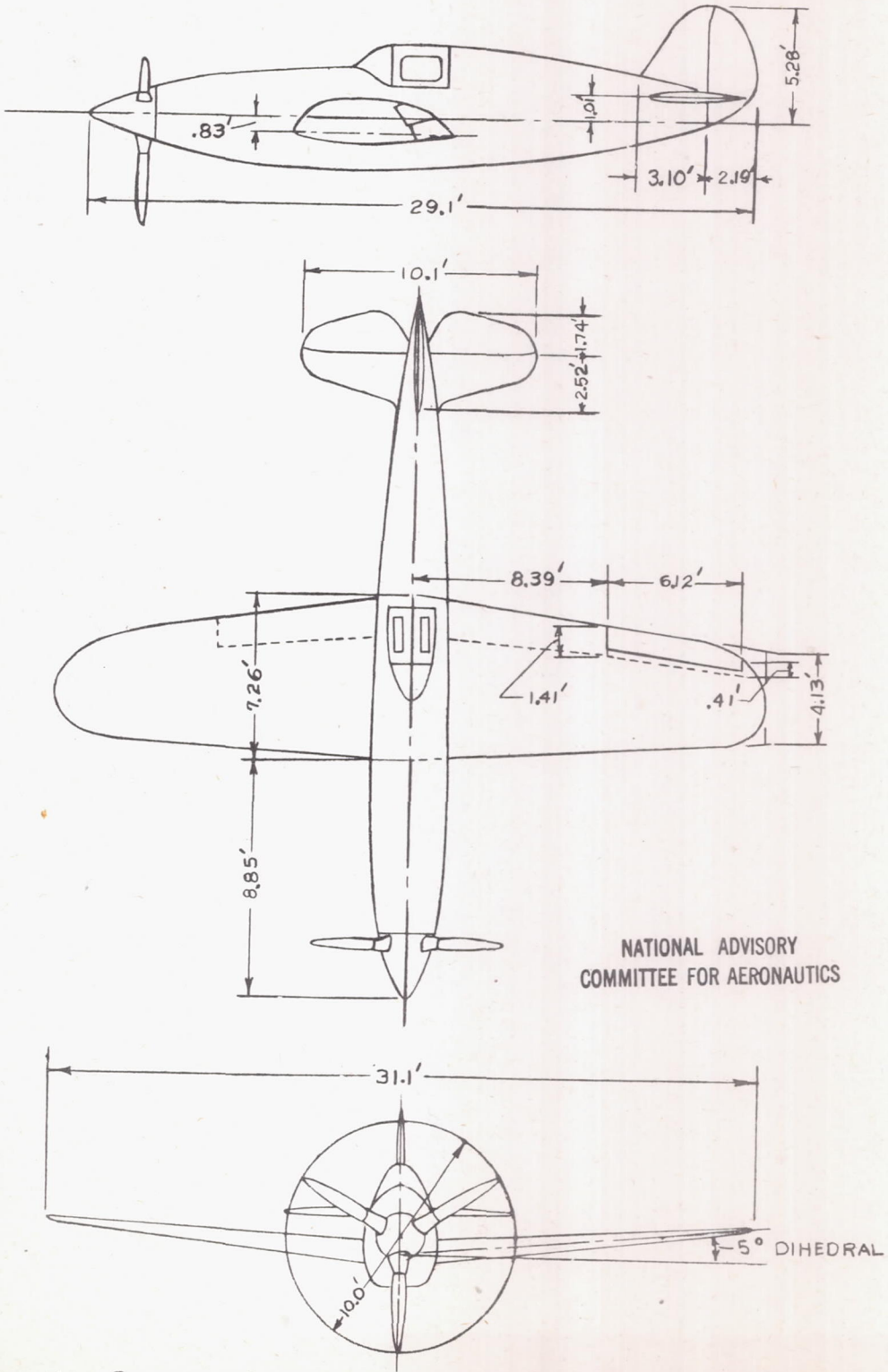

Figure 1.- General arrangement of wind-tunnel model, basic condition.

Section A

x	y_U	y_L
0	0	0
.116	.280	.250
.232	.390	.315
.463	.535	.405
.694	.645	.465
.925	.745	.510
1.487	.890	.565
1.850	.990	.595
2.315	1.065	.600
2.775	1.110	.595
3.700	1.135	.575
4.625	1.095	.540
5.560	1.000	.465
6.475	.840	.385
7.410	.625	.280
8.330	.360	.165
9.250	0	0

L.E. radius: 0.335
T.E. radius: 0.058

Section B

x	$y_U=y_L$
0	0
.194	.430
.388	.625
.775	.930
1.163	1.160
1.550	1.340
2.330	1.635
3.100	1.845
3.880	2.000
4.650	2.110
6.200	2.190
7.750	2.100
9.300	1.840
10.850	1.465
12.400	1.025
13.950	.535
15.500	0

L.E. radius: 0.520
T.E. radius: 0

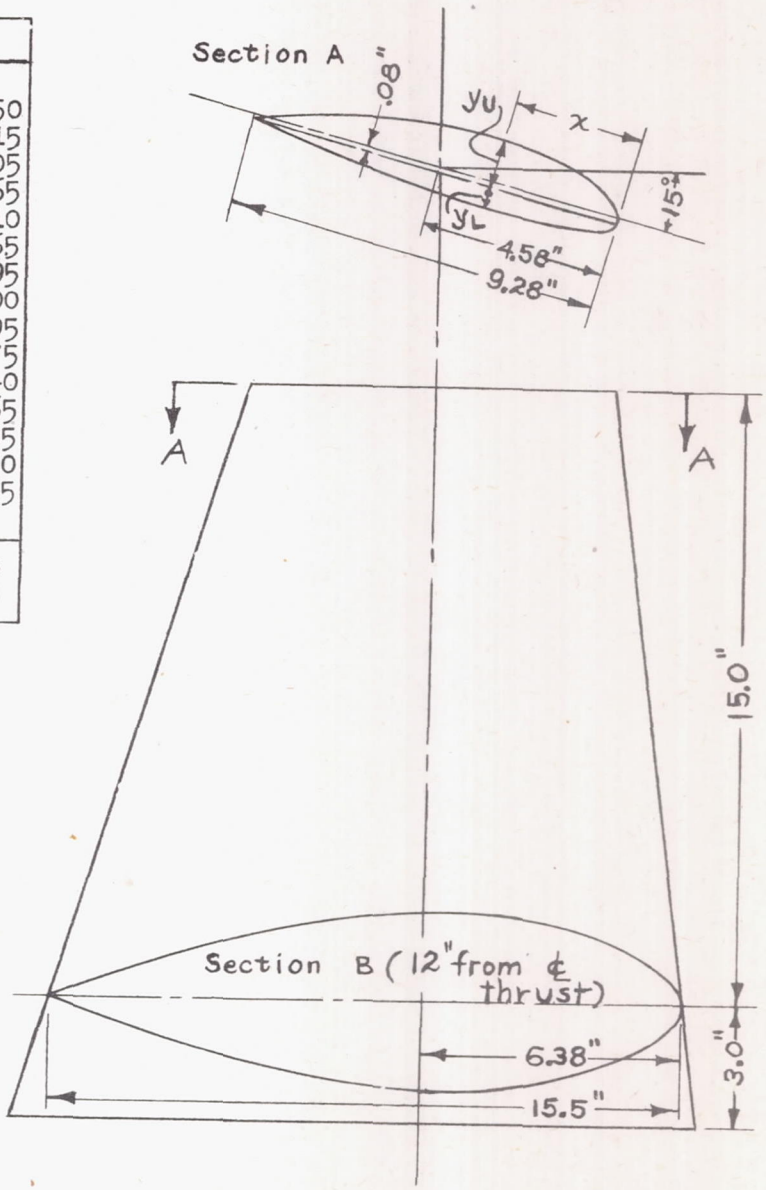

NATIONAL ADVISORY
COMMITTEE FOR AERONAUTICS

Figure 2.- Dimensions of propeller cuff.

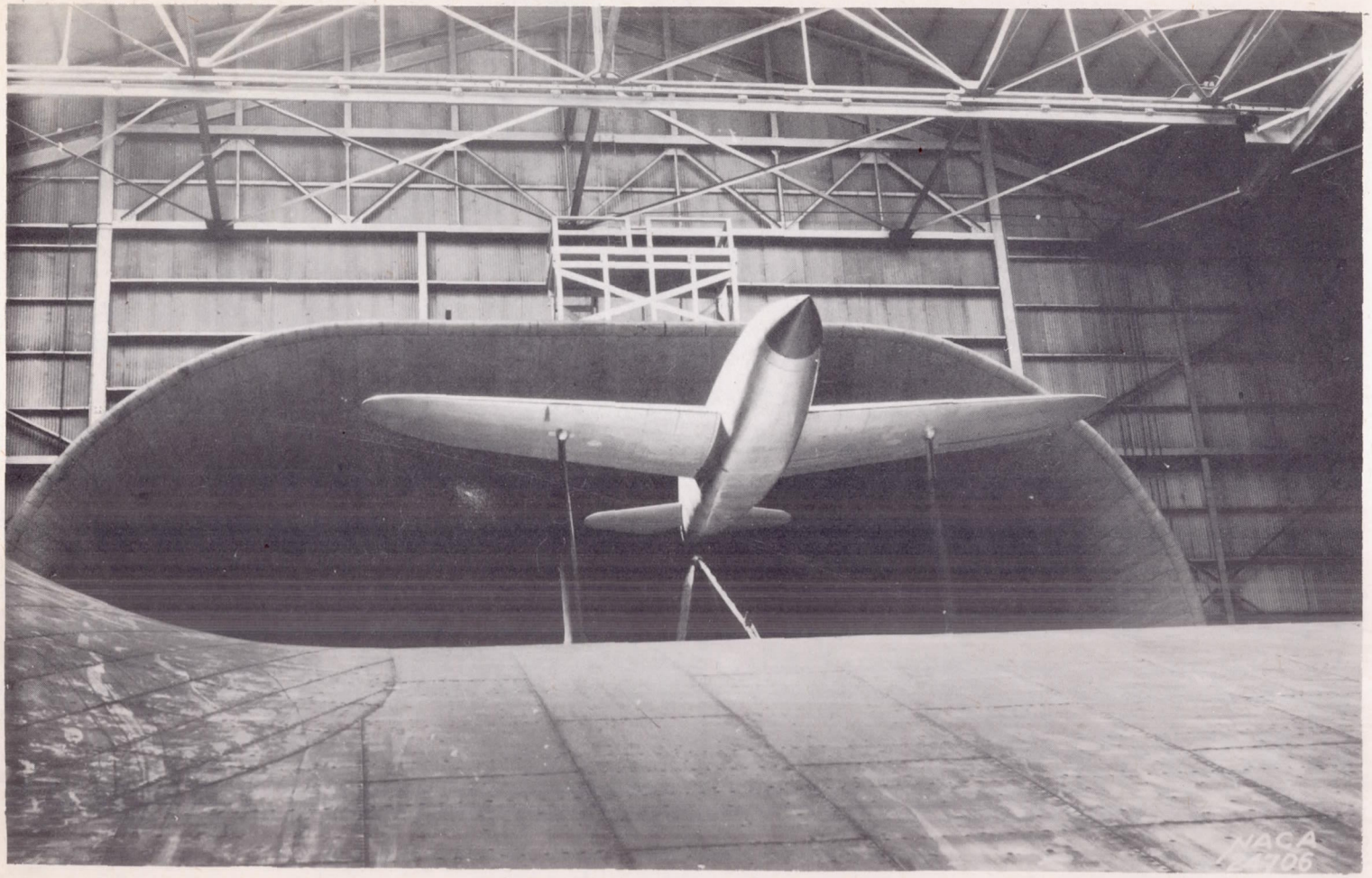

(a) Front view, propeller removed.

Figure 3.- Model in basic condition, mounted in the NACA full-scale tunnel.

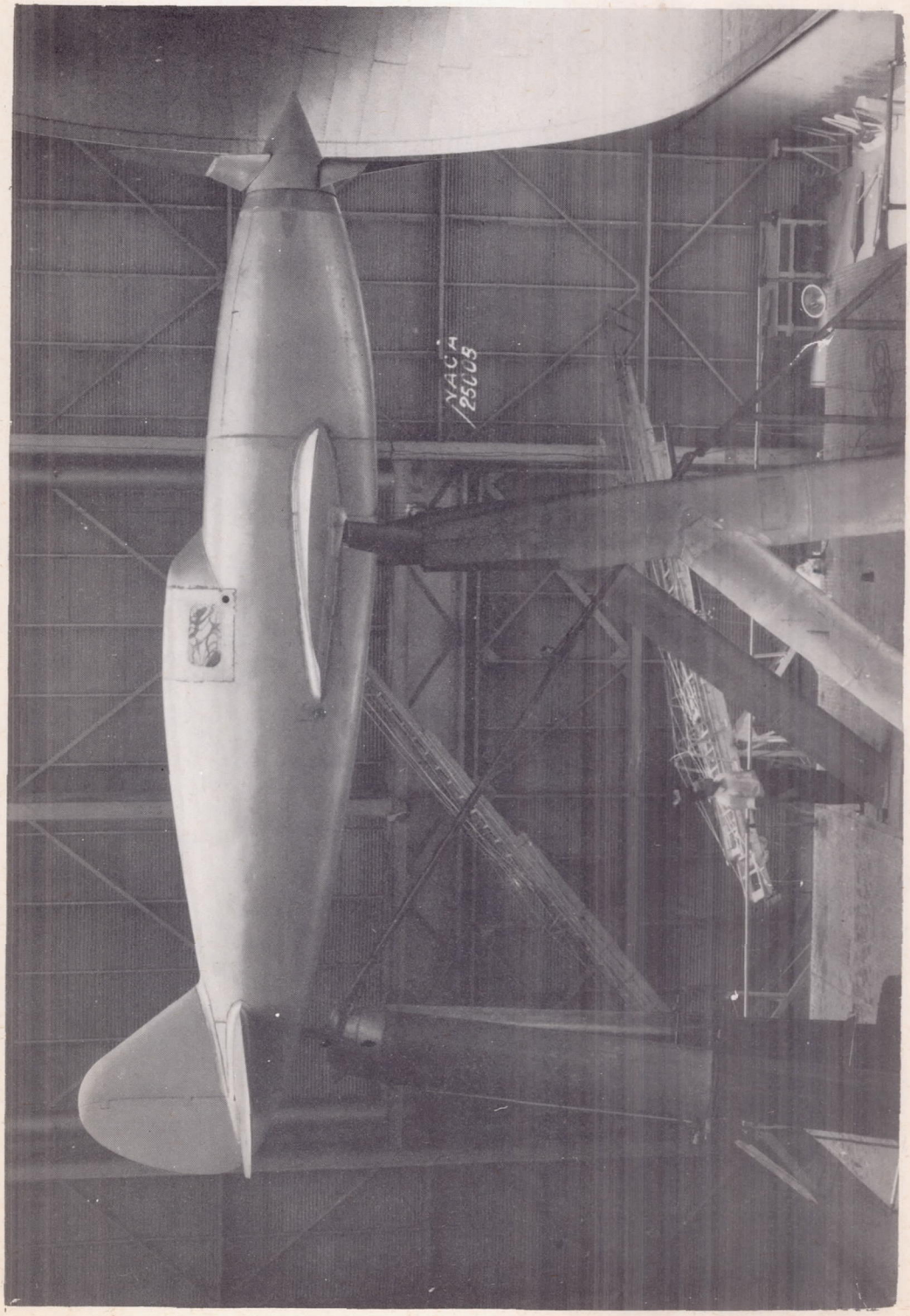

(b) Side view, propeller installed.

Figure 3.- Concluded.

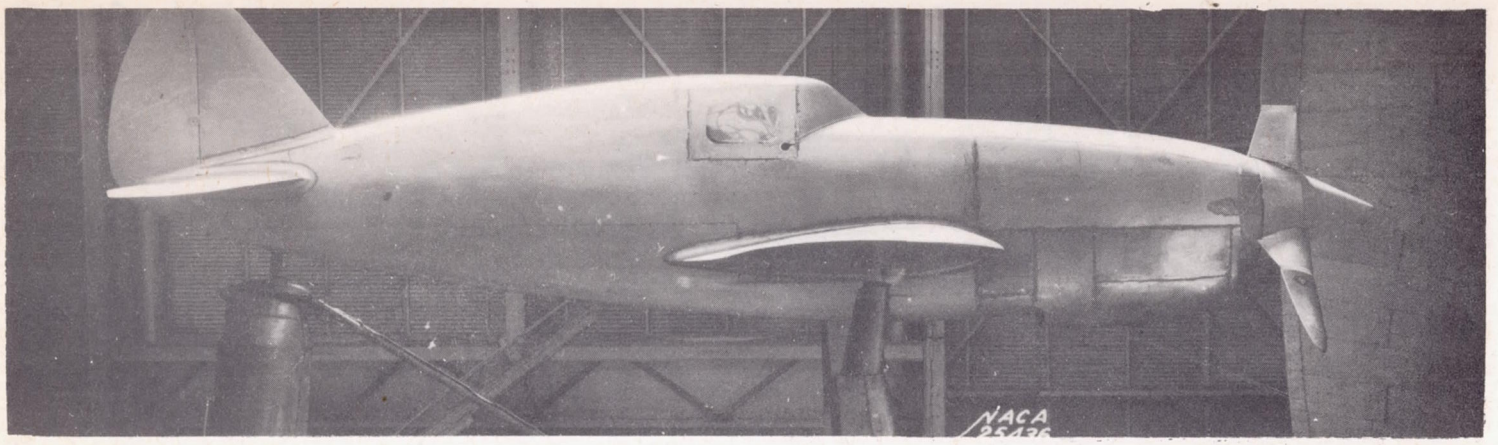

Figure 4.- Model with large forward underslung duct installed.

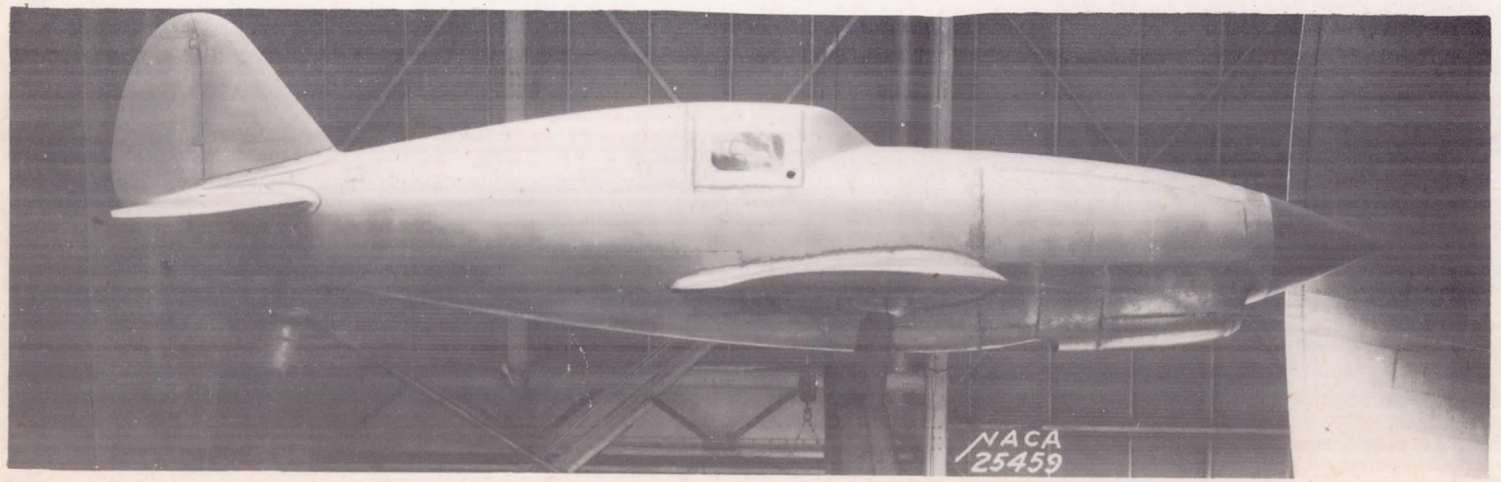

Figure 5.- Model with small forward underslung duct installed.

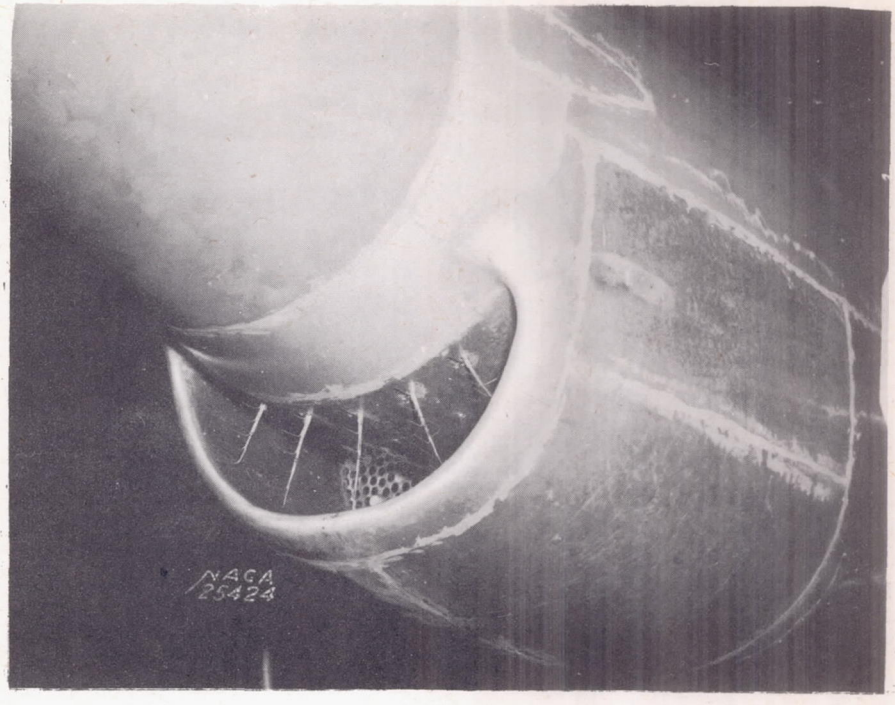

(a) Inlet.

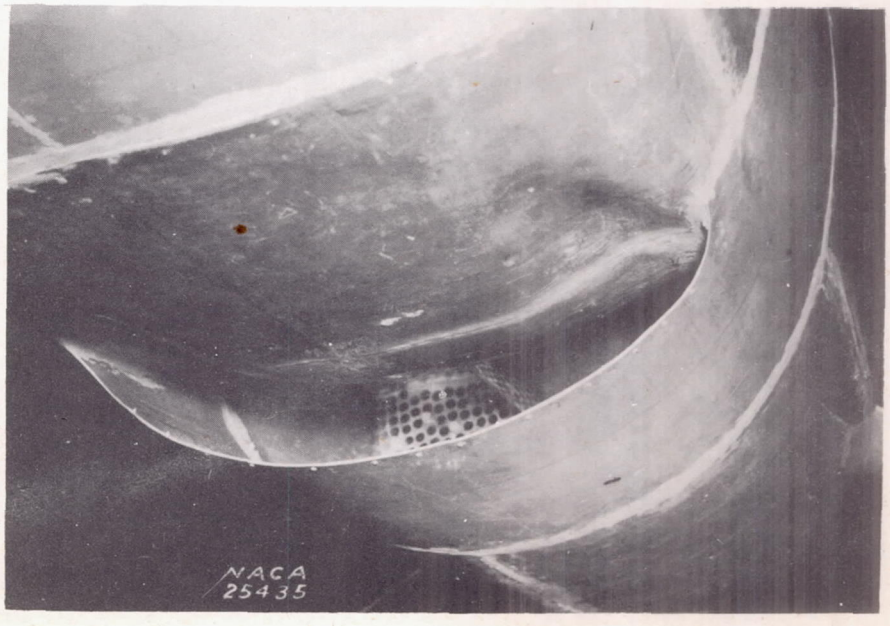

(b) Small outlet; exit flap off.

Figure 6.- Large forward underslung duct.

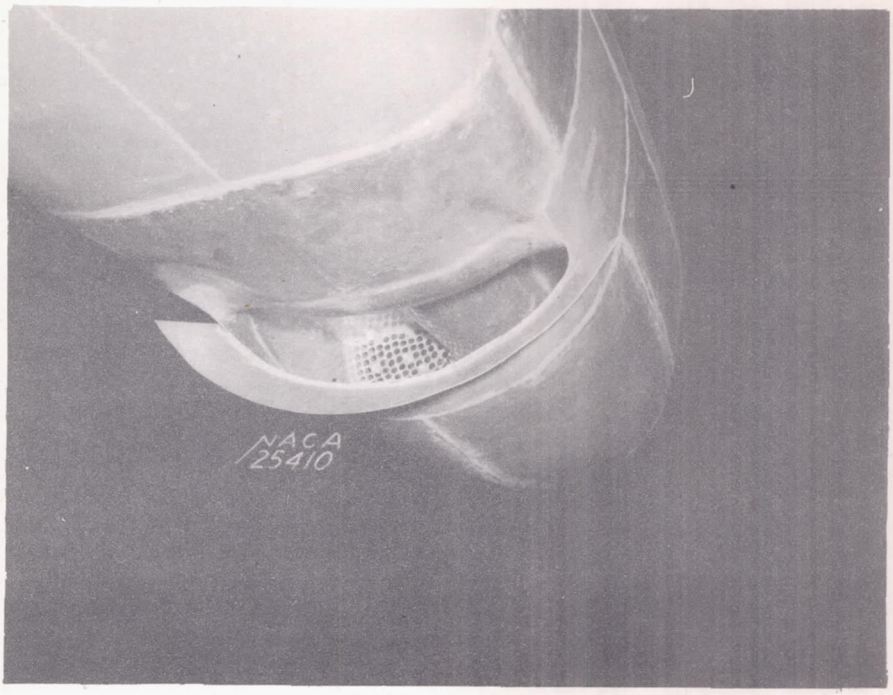

(c) Medium outlet; 45° exit flap installed.

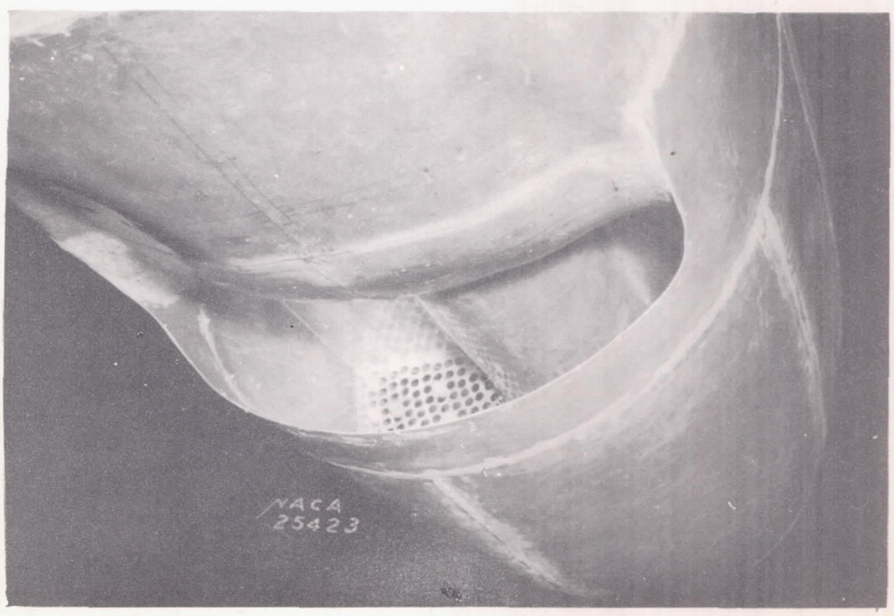

(d) Large outlet; exit flap off.

Figure 6.- Concluded.

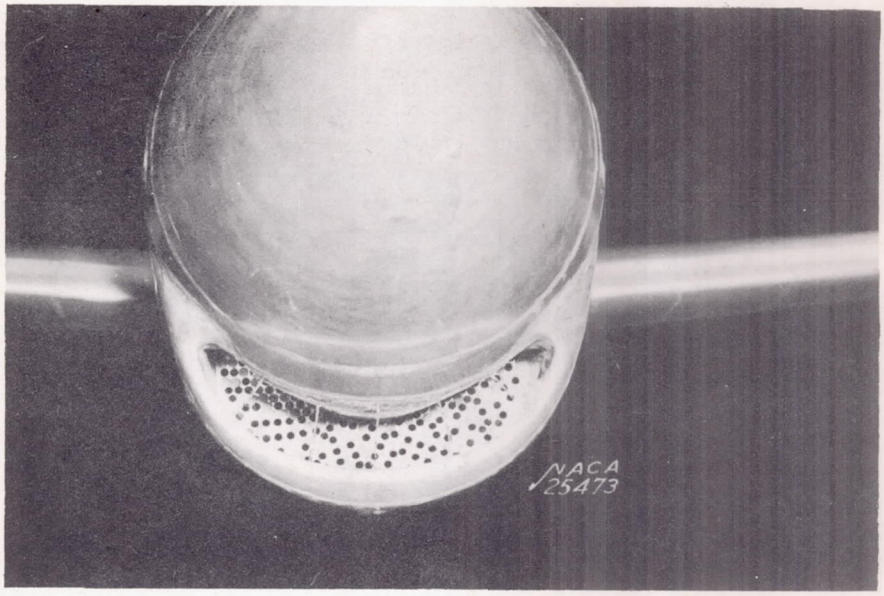

(a) Inlet.

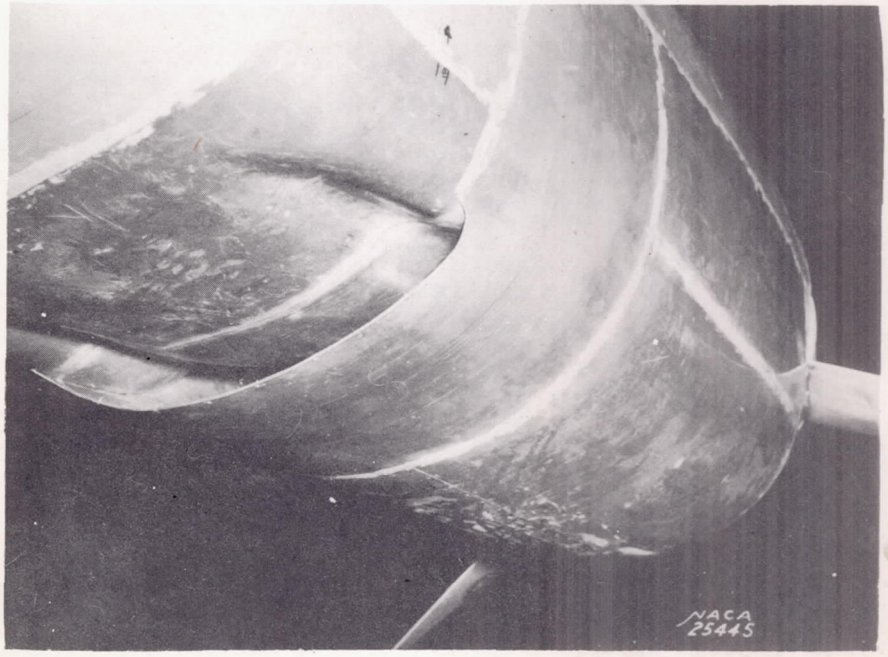

(b) Small outlet.

Figure 7.- Small forward underslung duct.

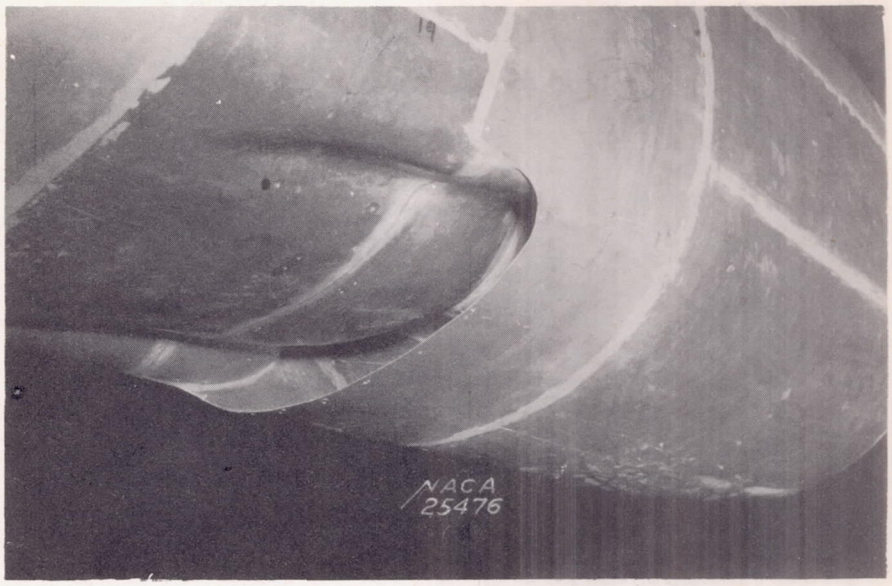

(c) Medium outlet.

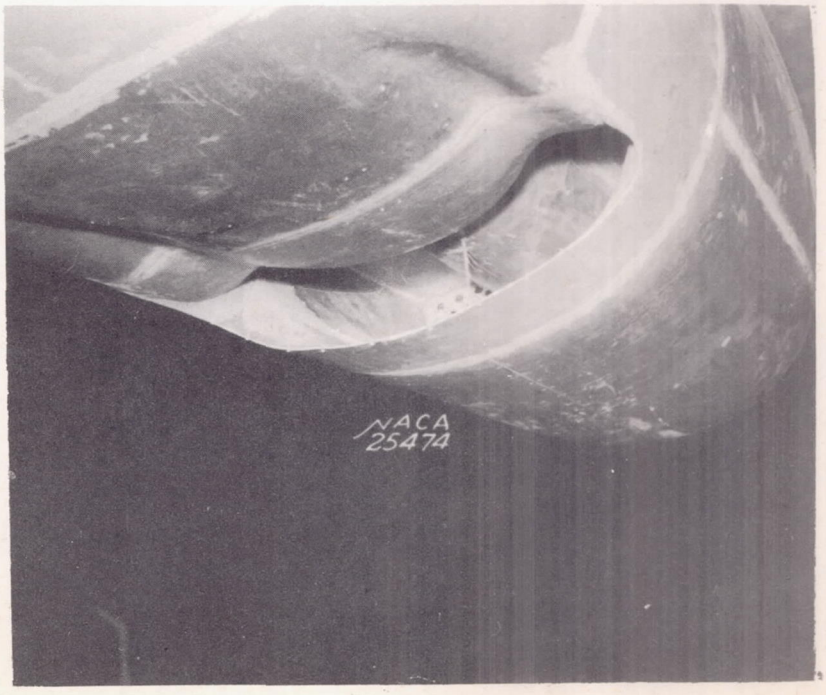

(d) Large outlet.

Figure 7.- Concluded.

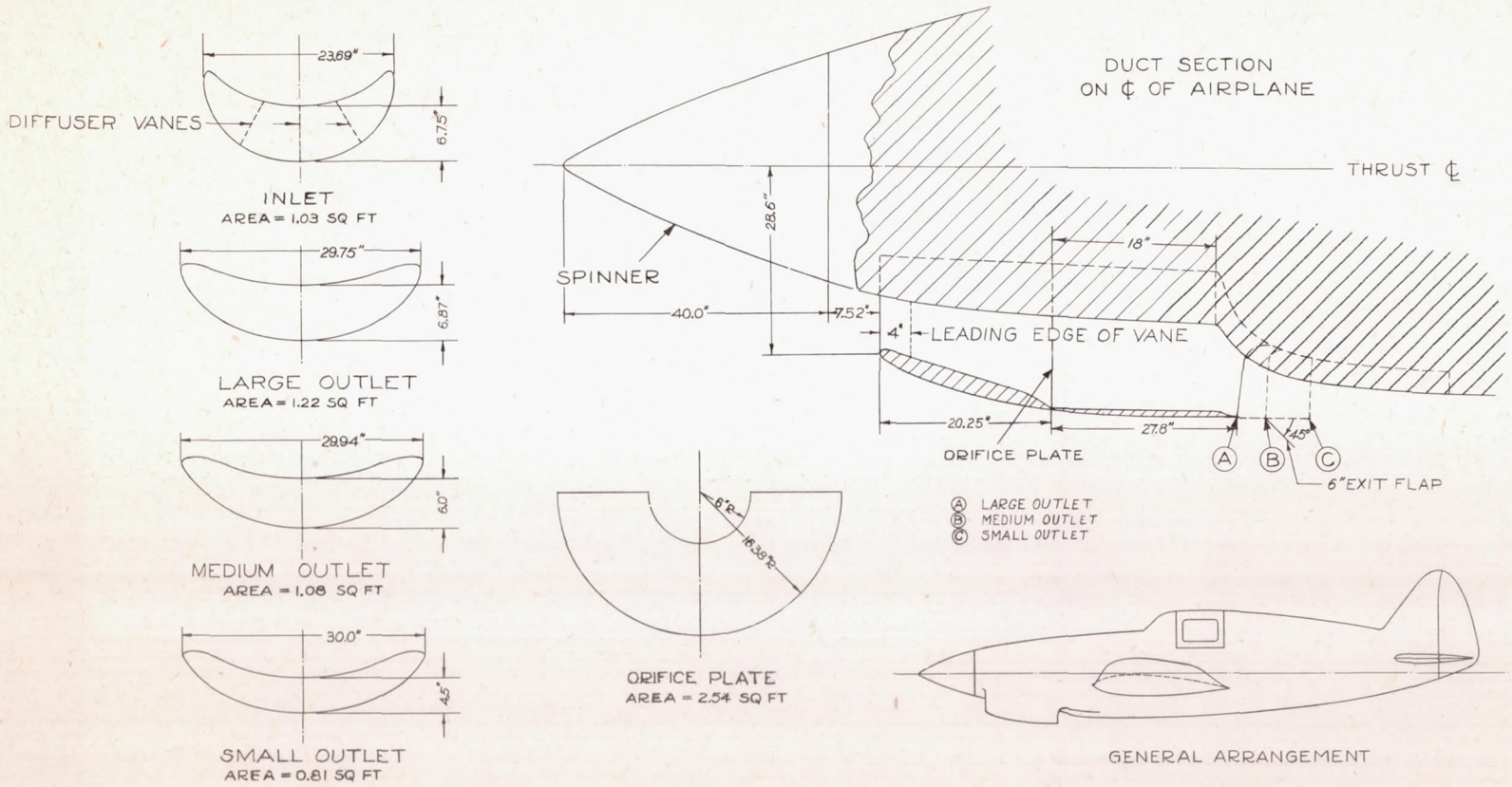

Figure 8.- Dimensions and arrangement of large forward underslung duct.

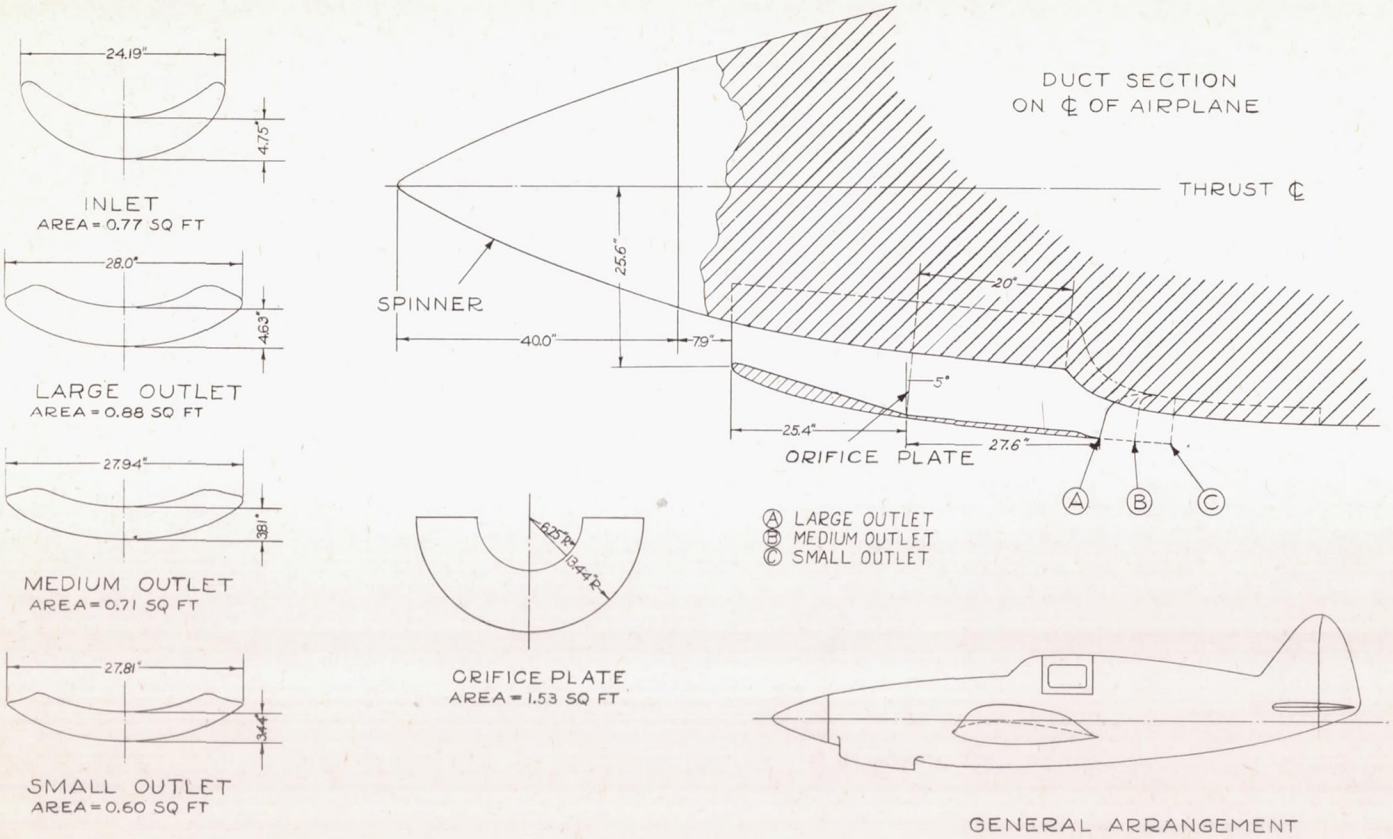

Figure 9.- Dimensions and arrangement of small forward underslung duct.

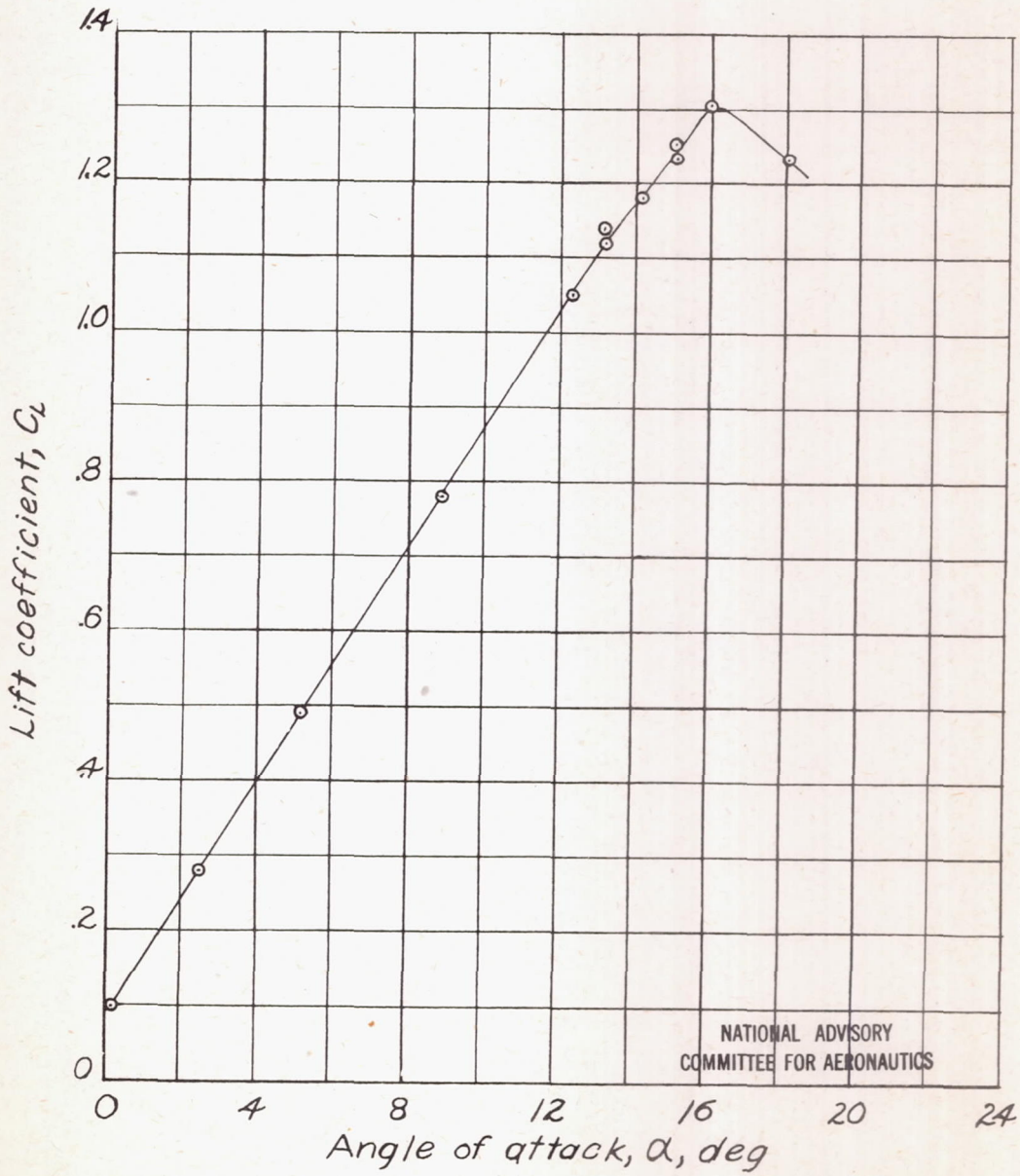

Figure 10. – Variation of lift coefficient with α.
Model in basic condition.

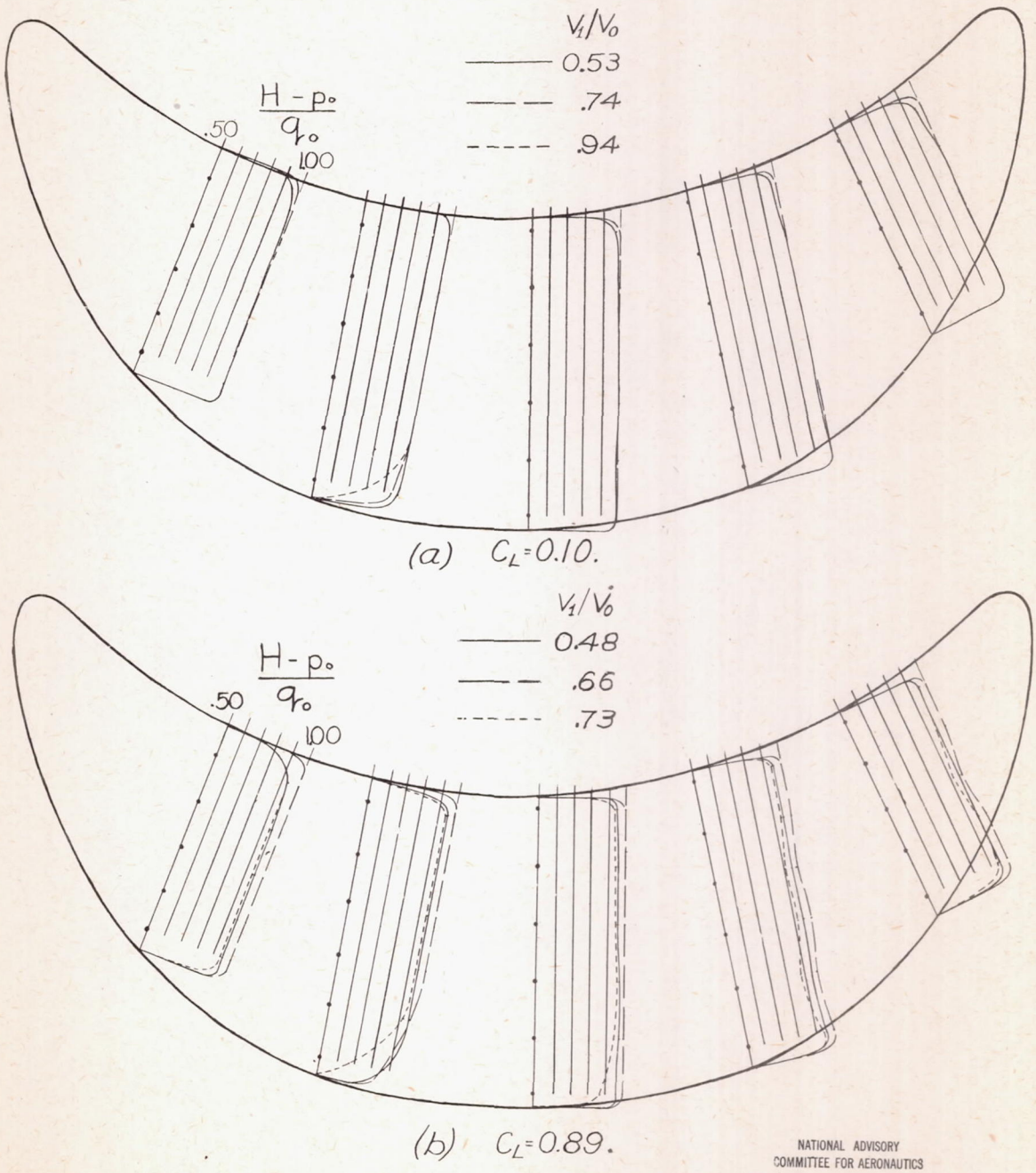

Figure 11.- Typical total-pressure distribution at inlet to large duct; propeller removed.

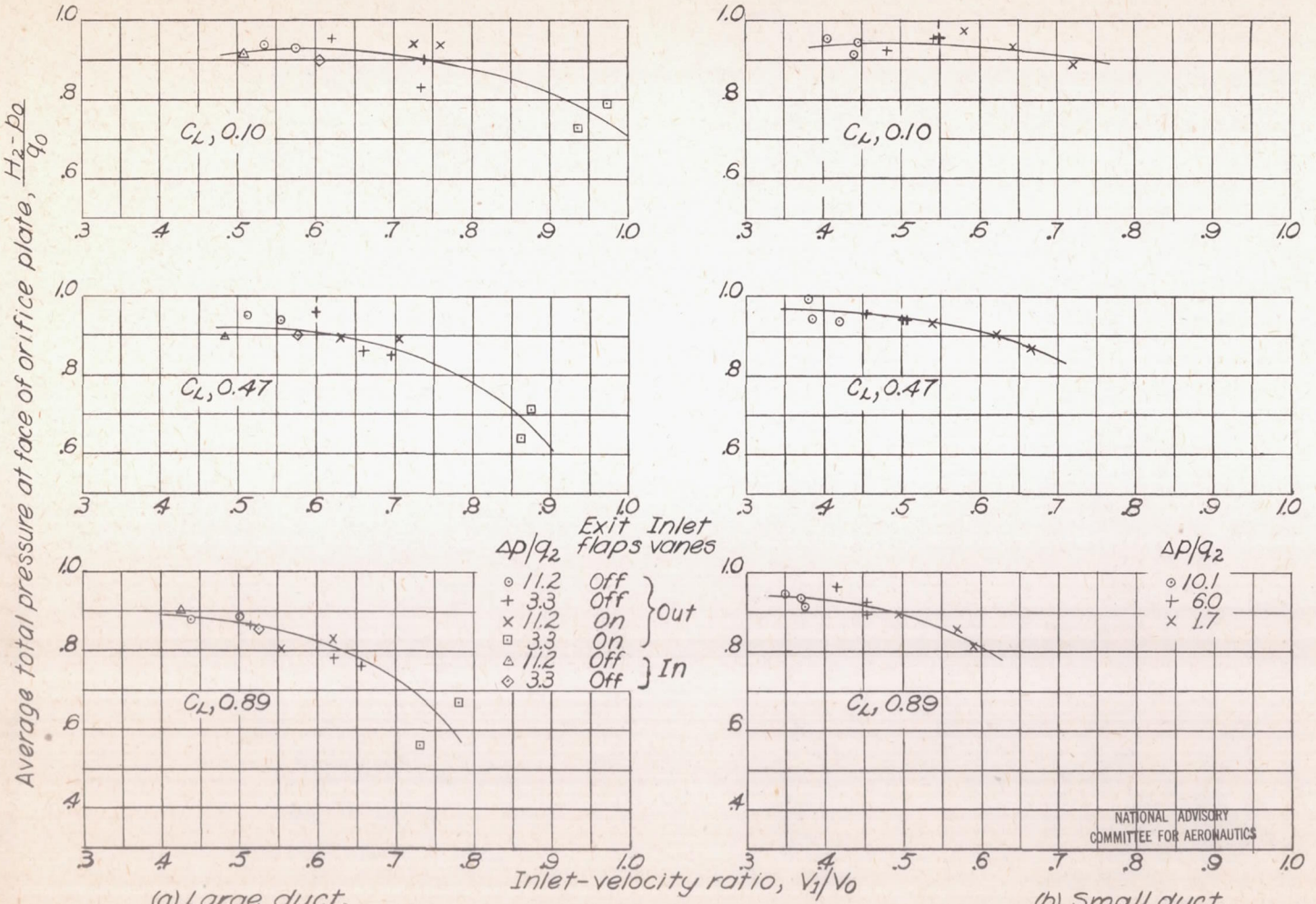

(a) Large duct. (b) Small duct.

Figure 12.- Variation of average total pressure at face of orifice plate with V_1/V_0. Large and small forward underslung ducts; propeller removed.

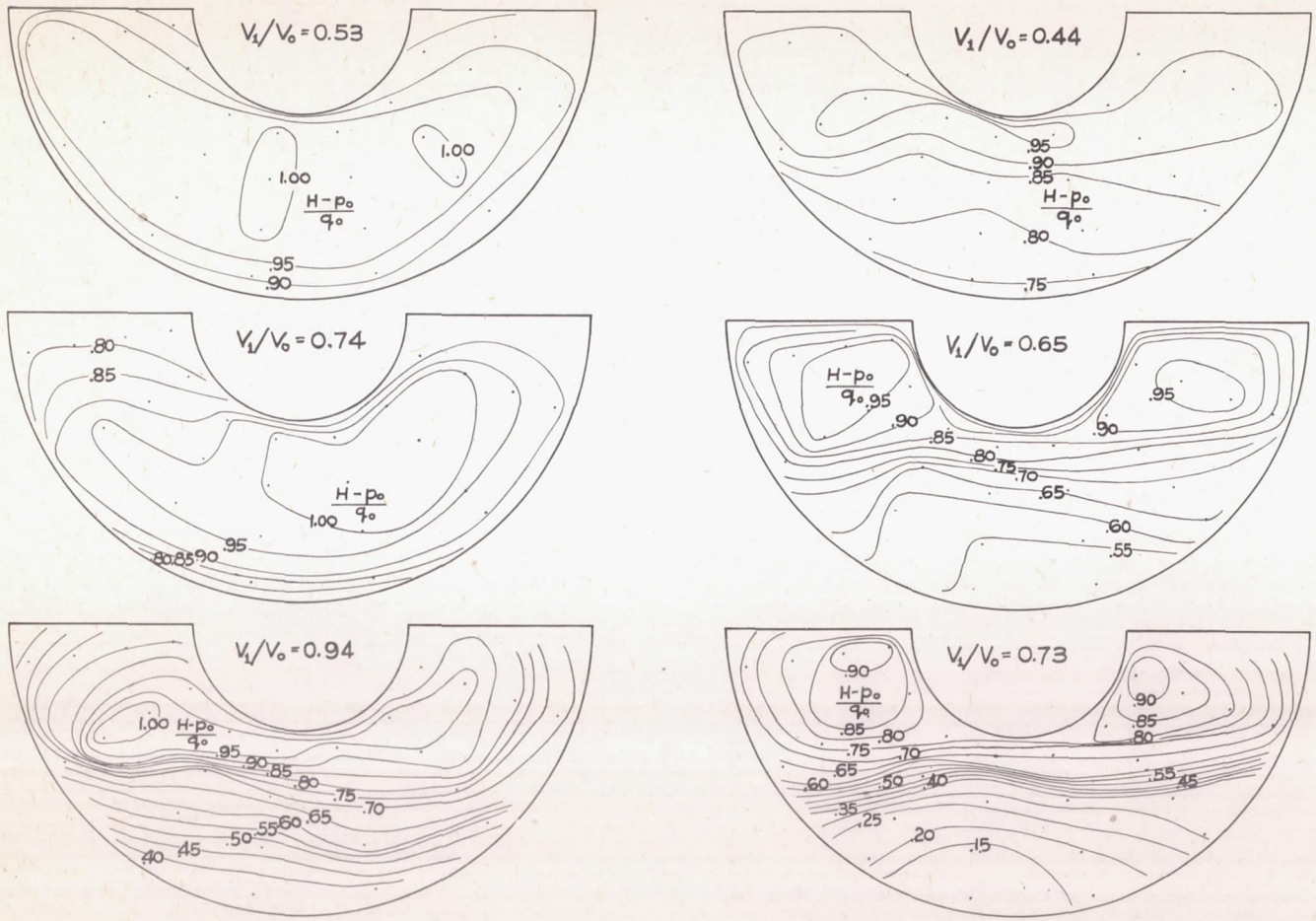

(a) $C_L = 0.10$.

(b) $C_L = 0.89$.

NATIONAL ADVISORY
COMMITTEE FOR AERONAUTICS

Figure 13.- Typical total-pressure distributions at face of orifice plate. Large forward underslung duct; propeller removed. (Dots represent tube locations.)

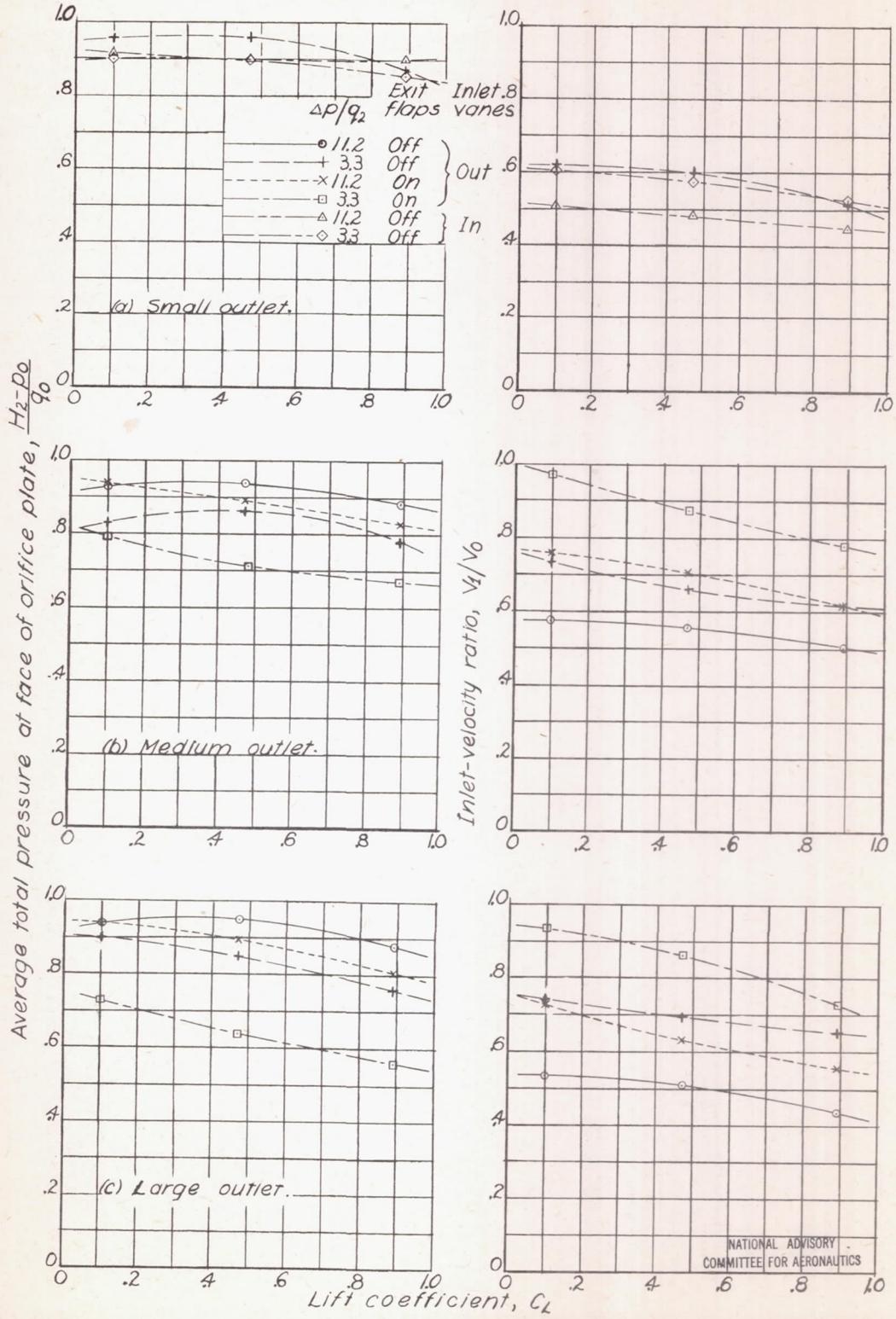

Figure 14.- Variation of average total pressure at face of orifice plate and inlet-velocity ratio with C_L. Large forward underslung duct; propeller removed.

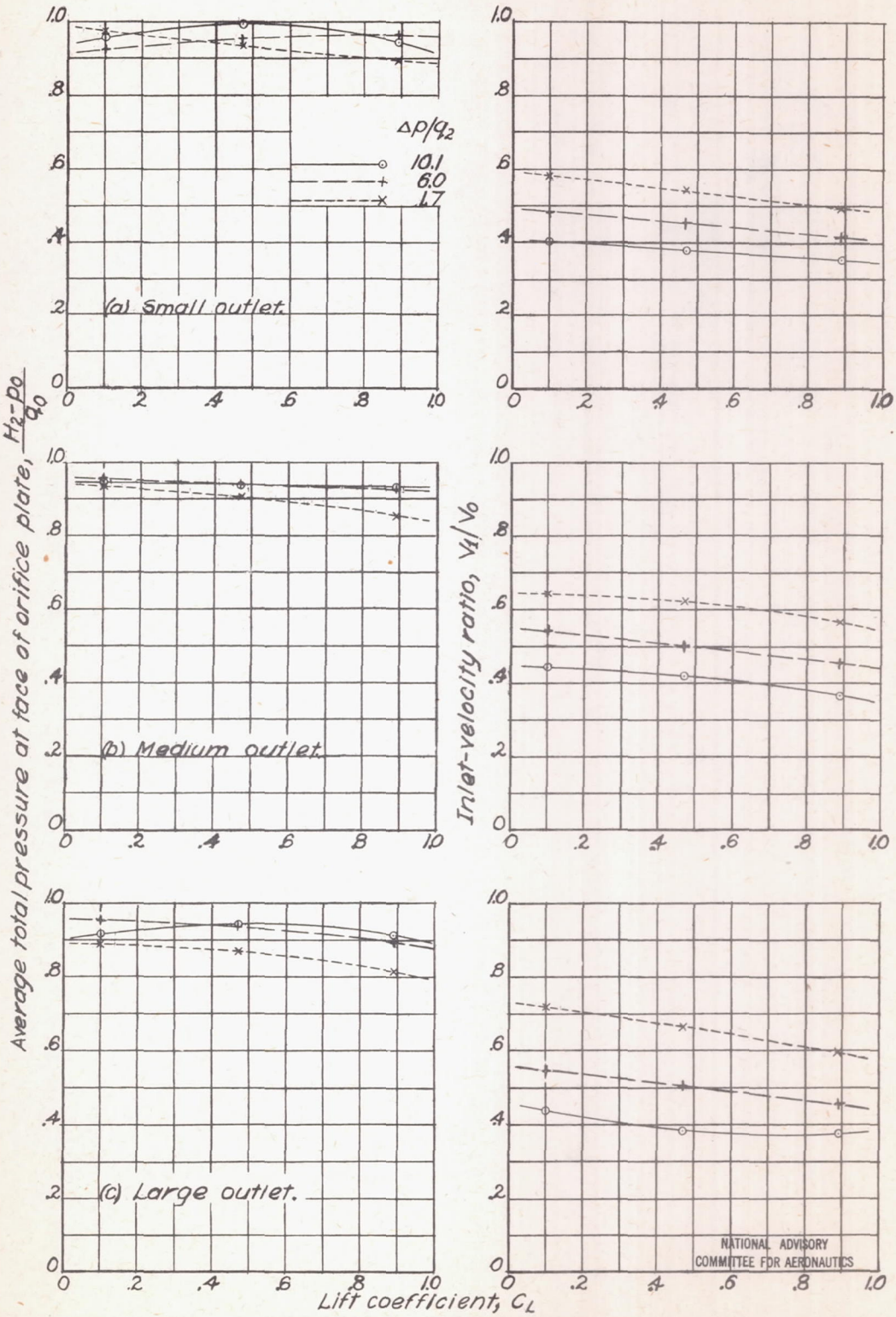

Figure 15.- Variation of average total pressure at face of orifice plate and inlet-velocity ratio with C_L. Small forward underslung duct; propeller removed.

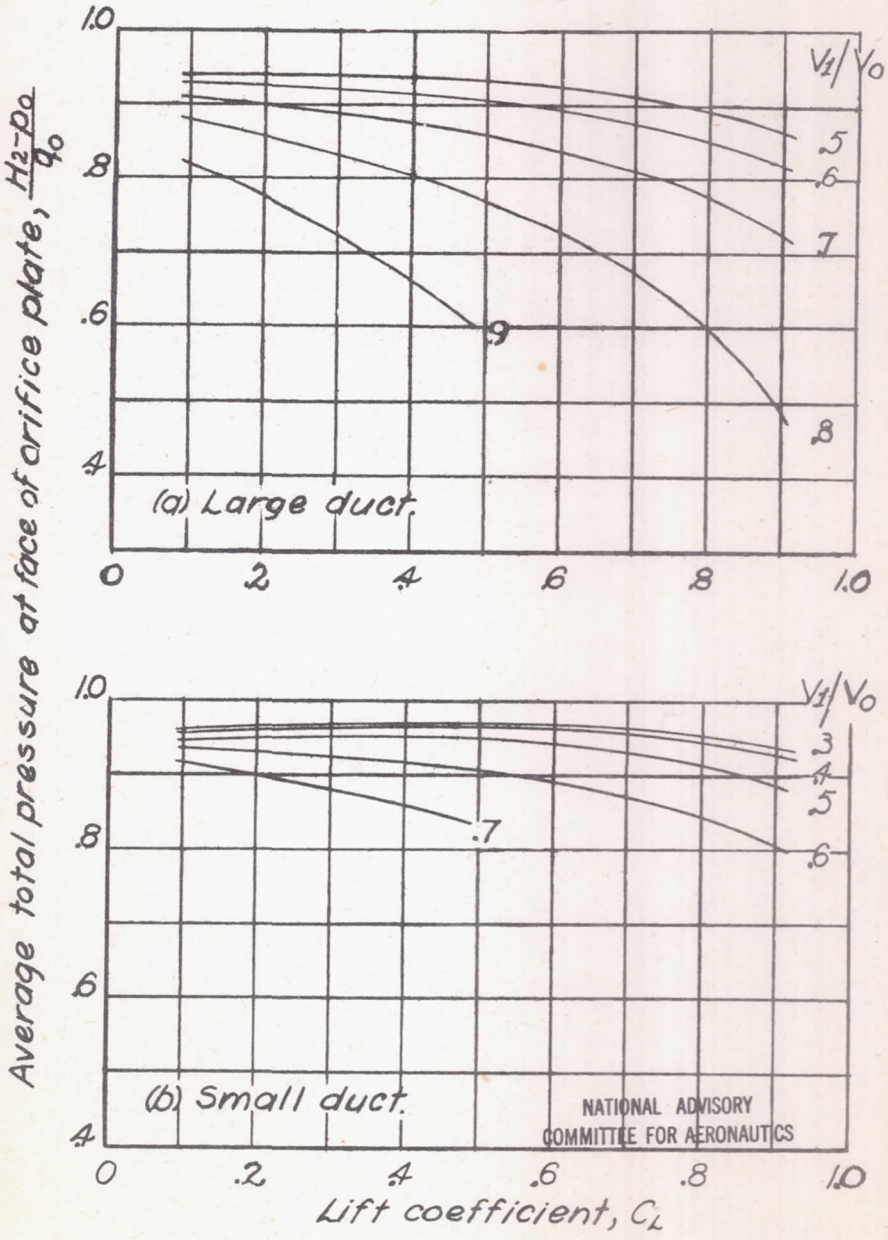

Figure 16.- Variation of average total pressure at face of orifice plate with C_L. Large and small forward underslung ducts; propeller removed.

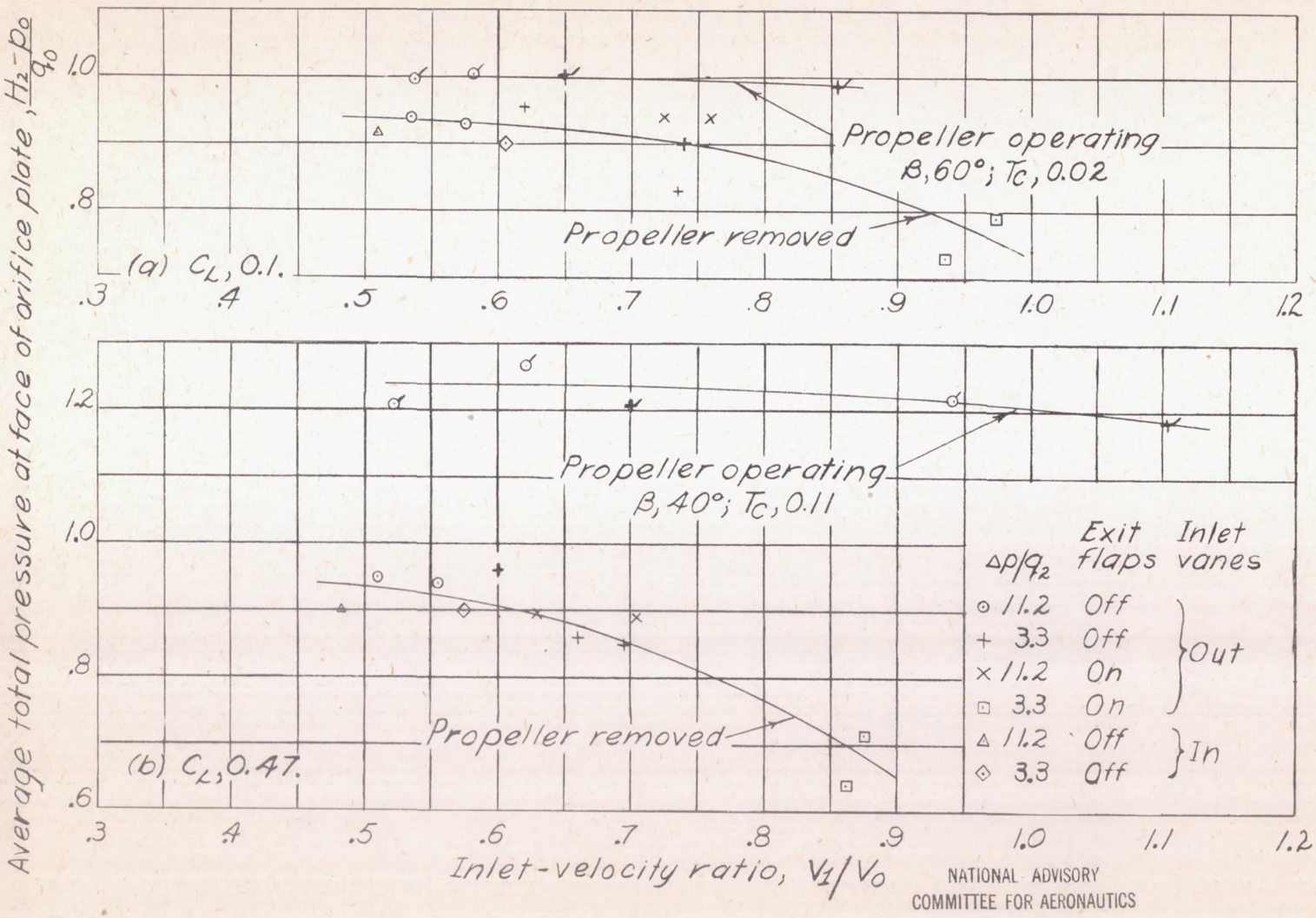

Figure 17.- Effect of propeller operation on the variation of total pressure at face of orifice plate with V_1/V_0. Large forward underslung duct. (Flagged symbols for propeller operating.)

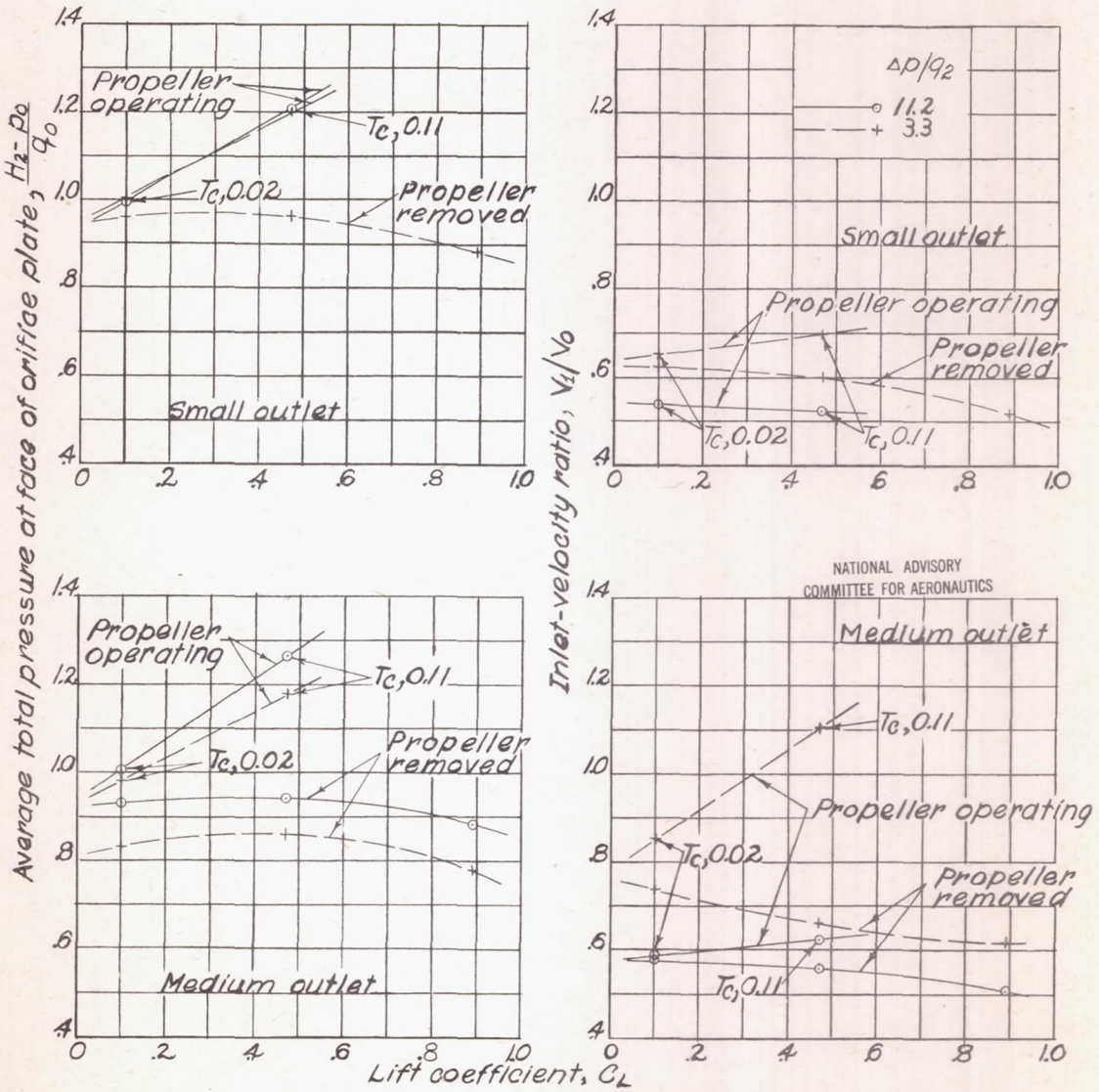

Figure 18.- Effect of propeller operation on the variation of average total pressure at face of orifice plate and inlet-velocity ratio with C_L. Large forward underslung duct; normal rated power.

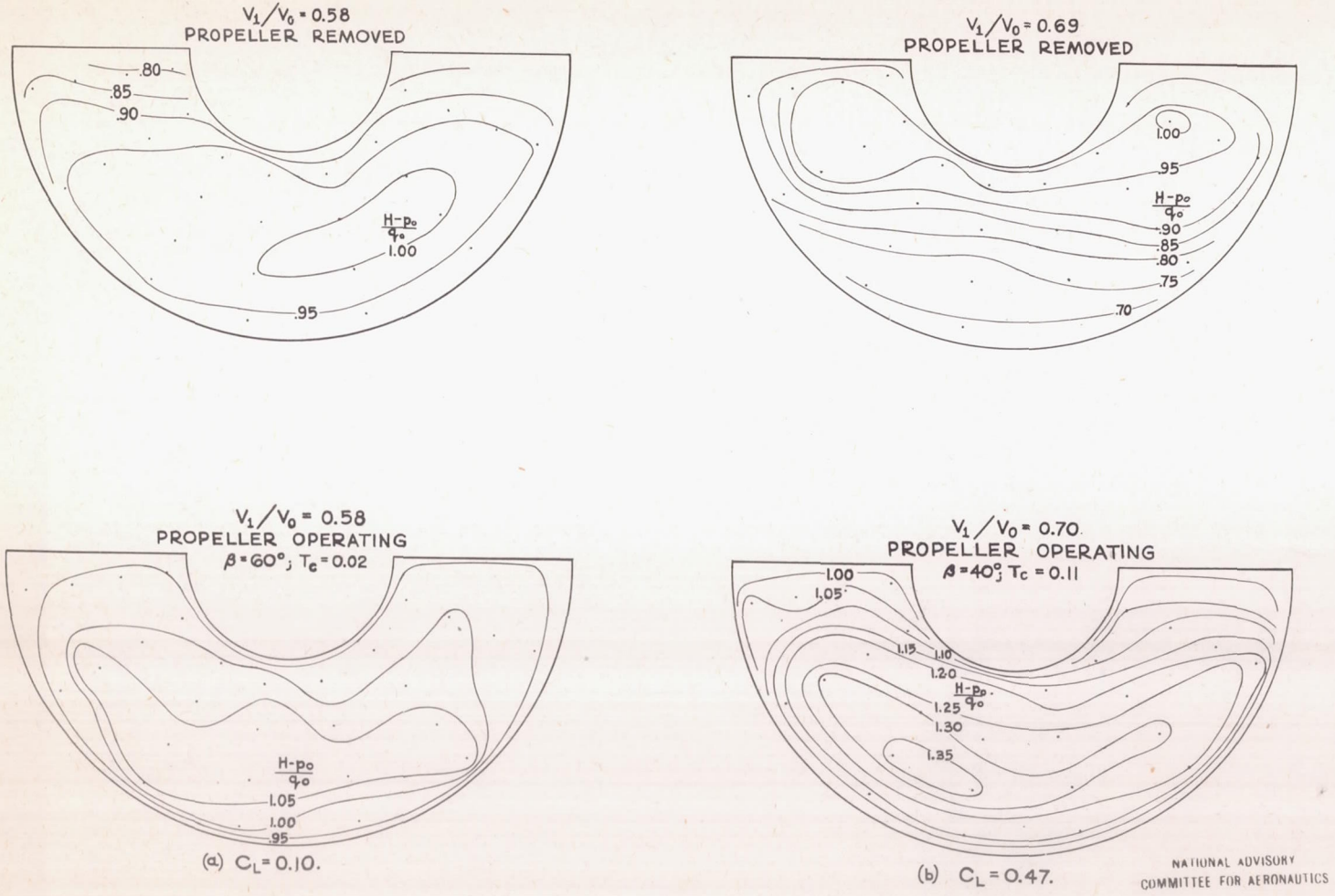

Figure 19.- Effect of propeller operation on total-pressure distributions at face of orifice plate. Large forward underslung duct. (Dots represent tube locations.)

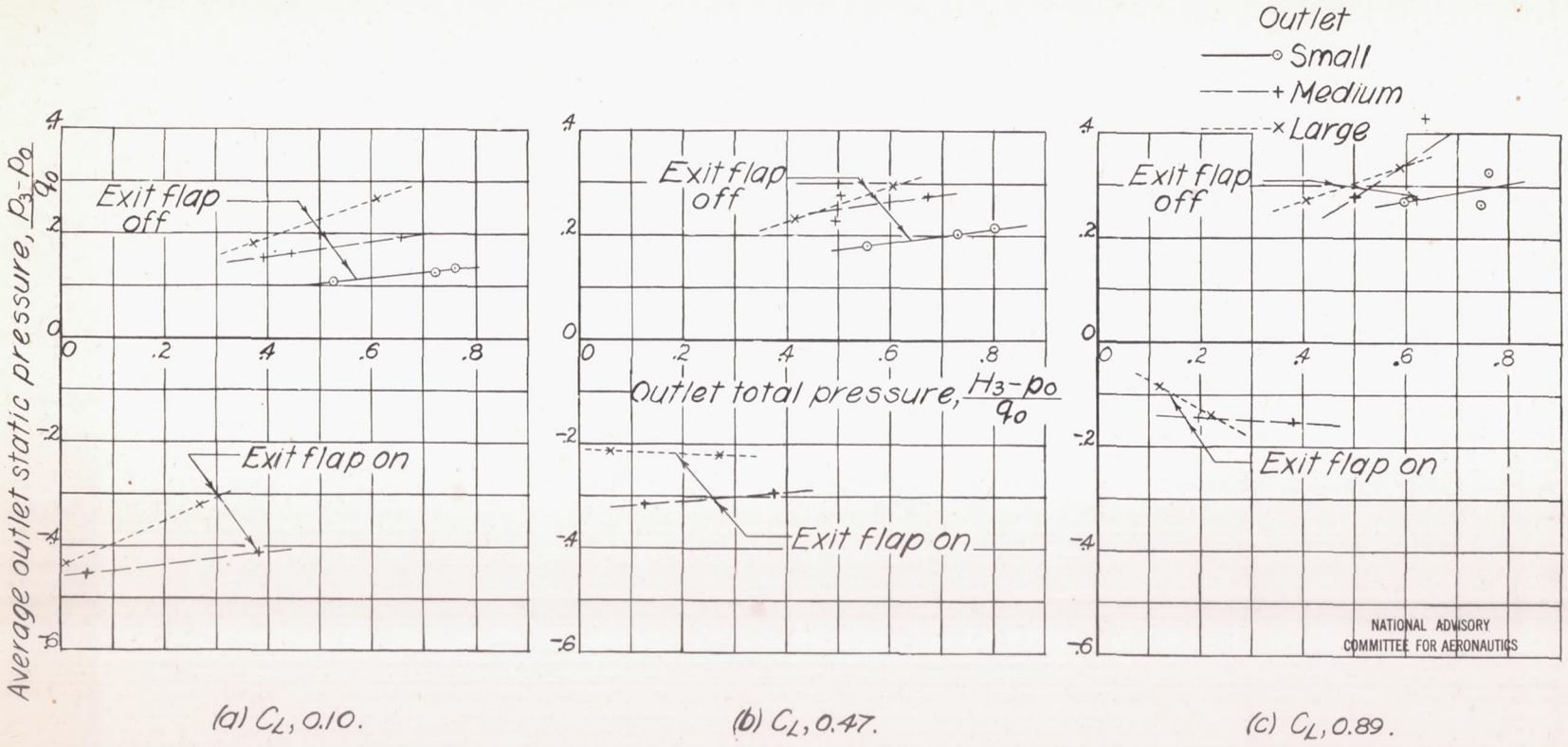

(a) C_L, 0.10. (b) C_L, 0.47. (c) C_L, 0.89.

Figure 20.– Variation of outlet static pressure with outlet total pressure. Large forward underslung duct; propeller removed.

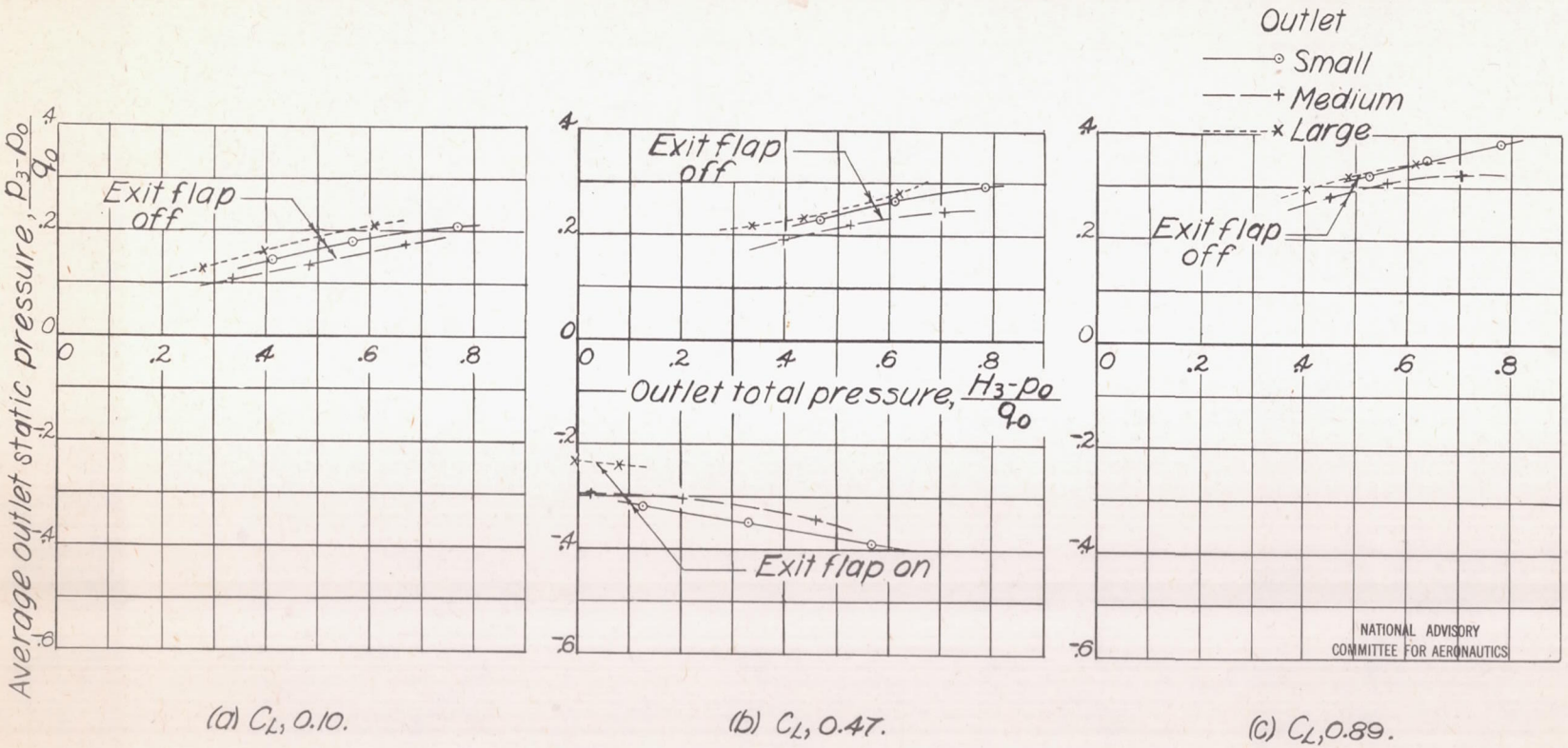

(a) C_L, 0.10. (b) C_L, 0.47. (c) C_L, 0.89.

Figure 21. – Variation of outlet static pressure with outlet total pressure. Small forward underslung duct; propeller removed.

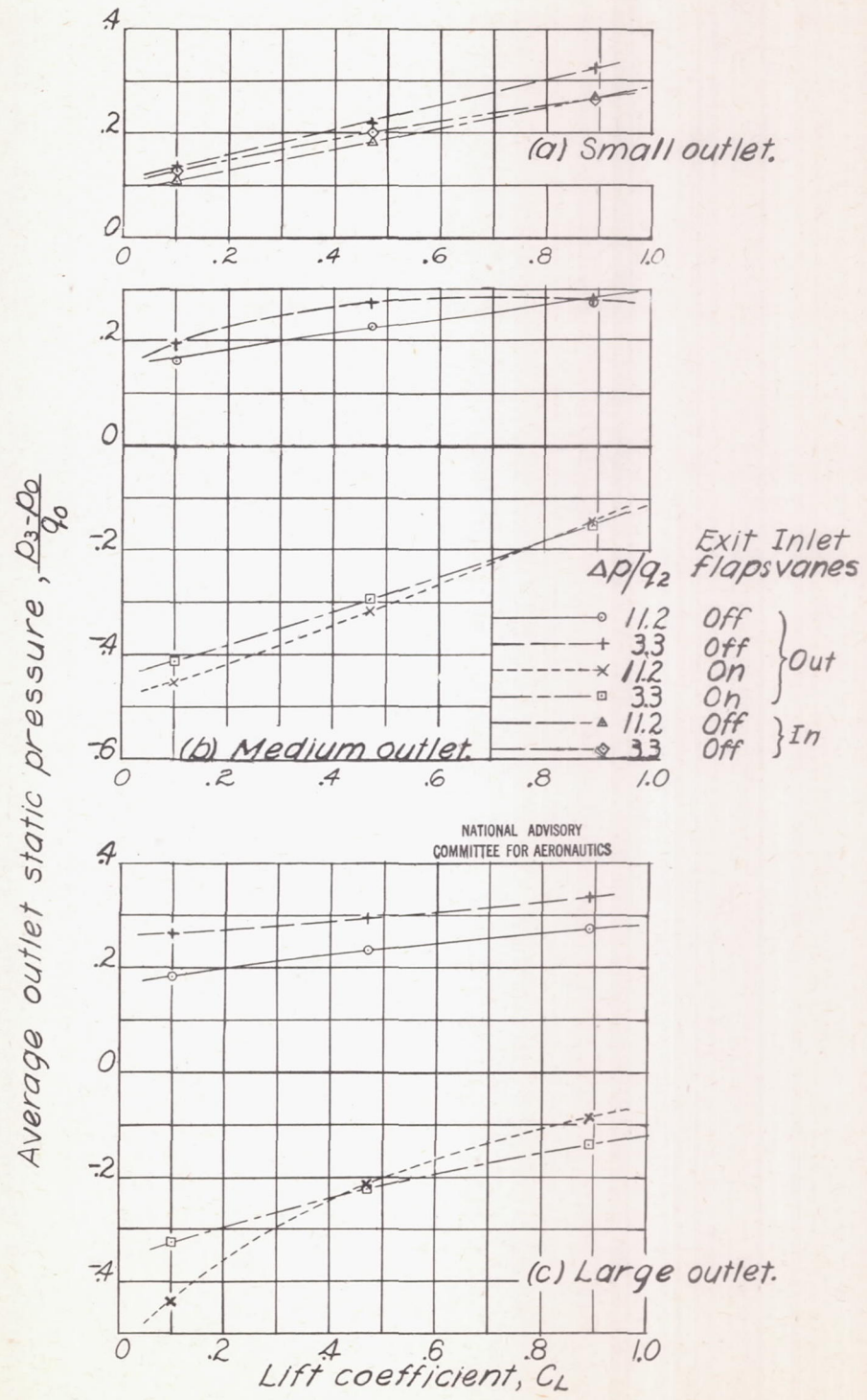

Figure 22.- Variation of average outlet static pressure with C_L. Large forward underslung duct; propeller removed.

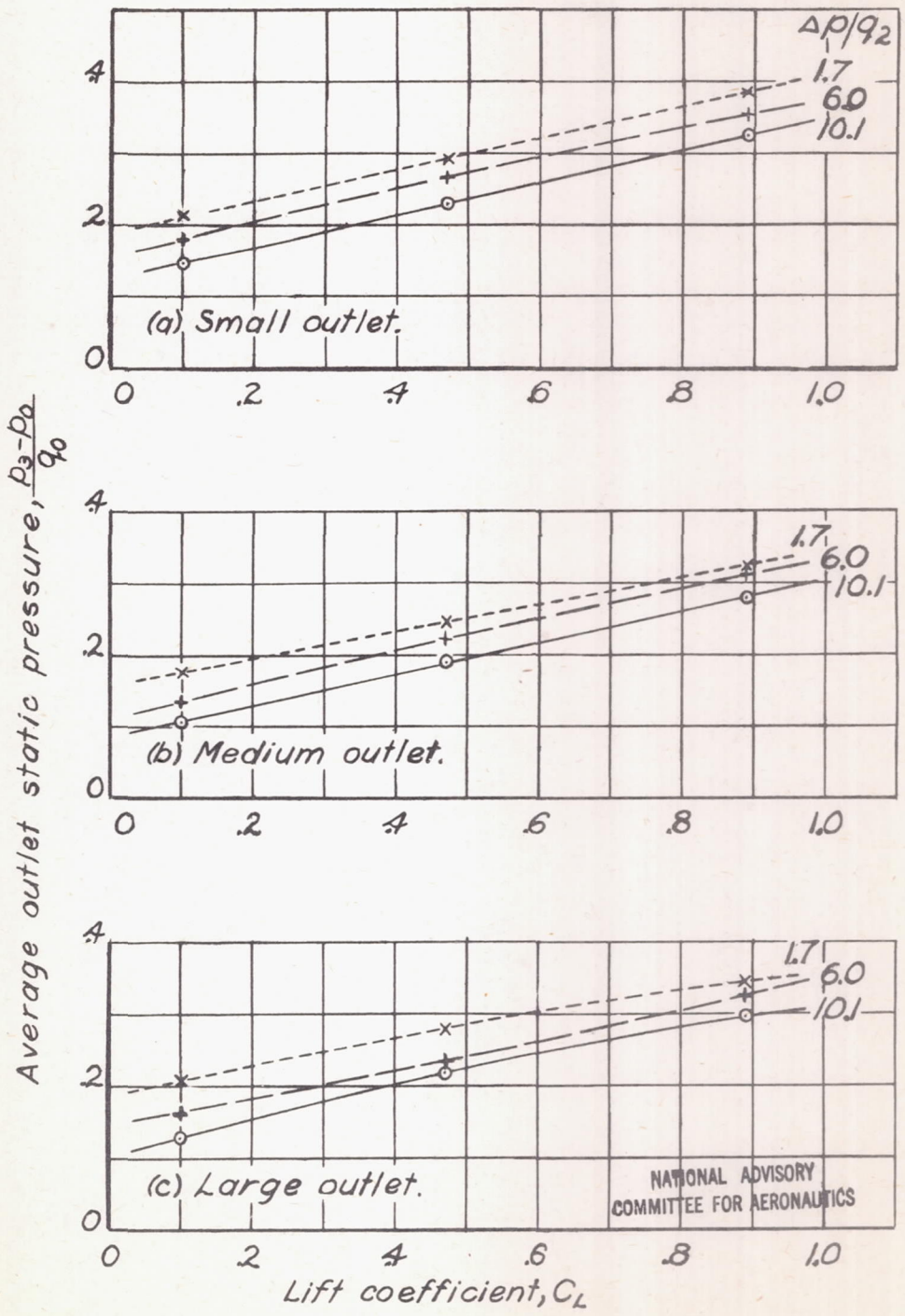

Figure 23.- Variation of average outlet static pressure with C_L. Small forward underslung duct; propeller removed.

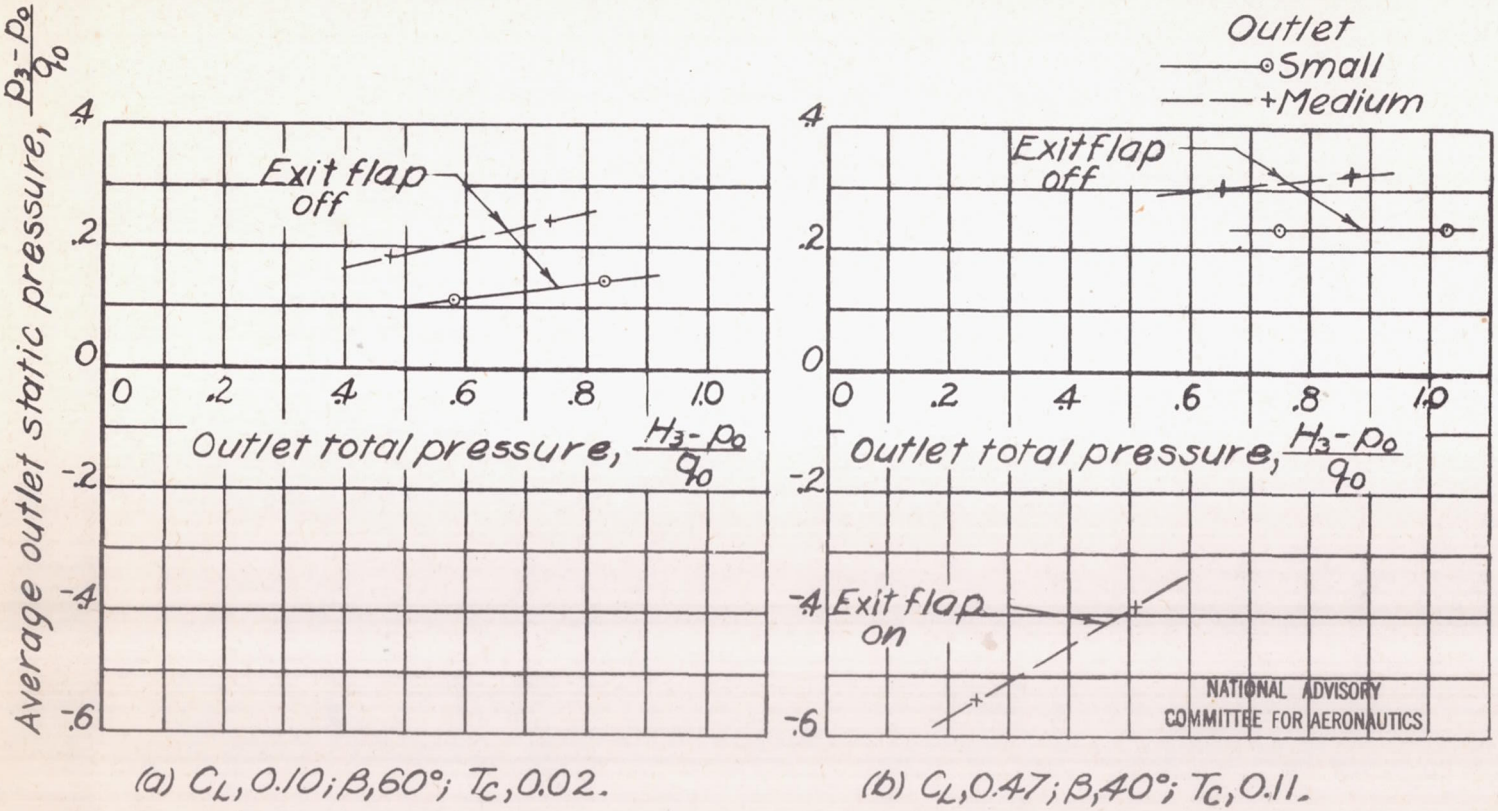

(a) C_L, 0.10; β, 60°; T_c, 0.02.

(b) C_L, 0.47; β, 40°; T_c, 0.11.

Figure 24.- Variation of outlet static pressure with outlet total pressure. Large forward underslung duct; propeller operating.

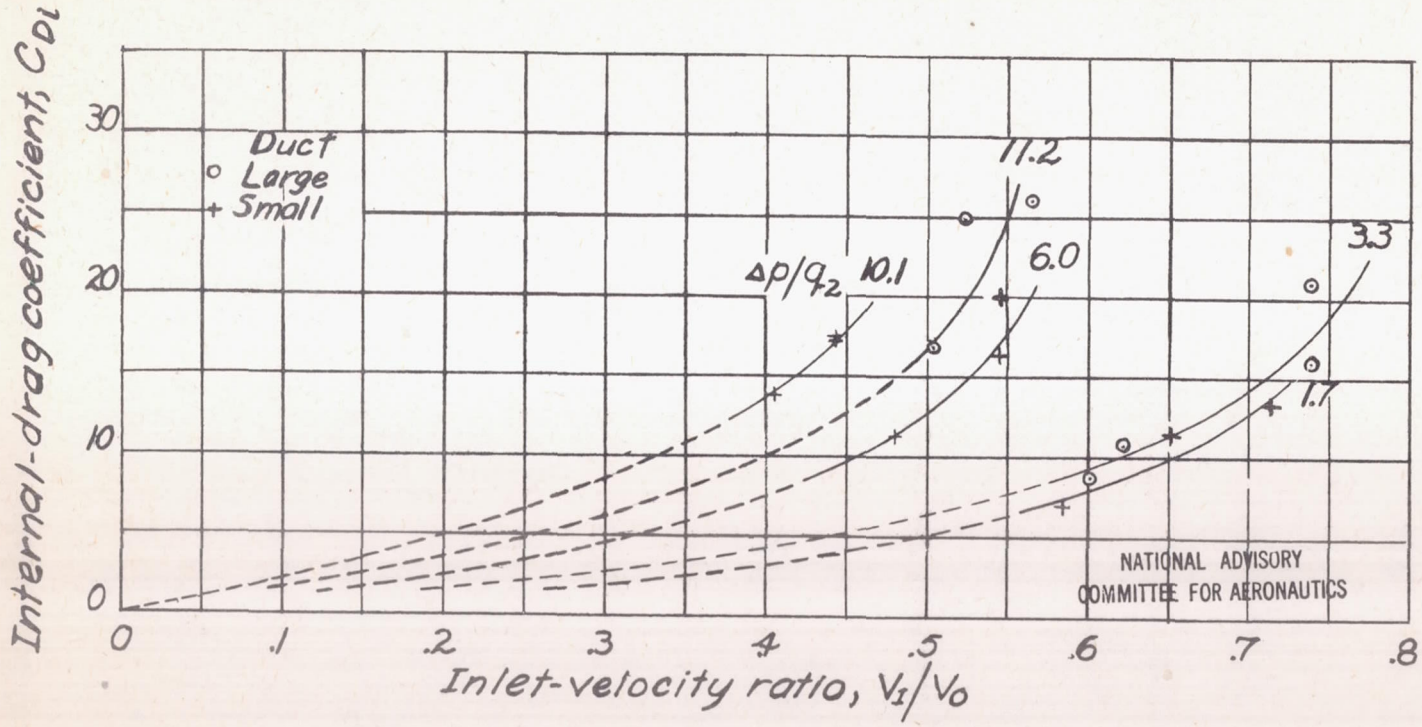

Figure 25.–Variation of internal-drag coefficient with V_i/V_0. Large and small forward underslung ducts; propeller removed.

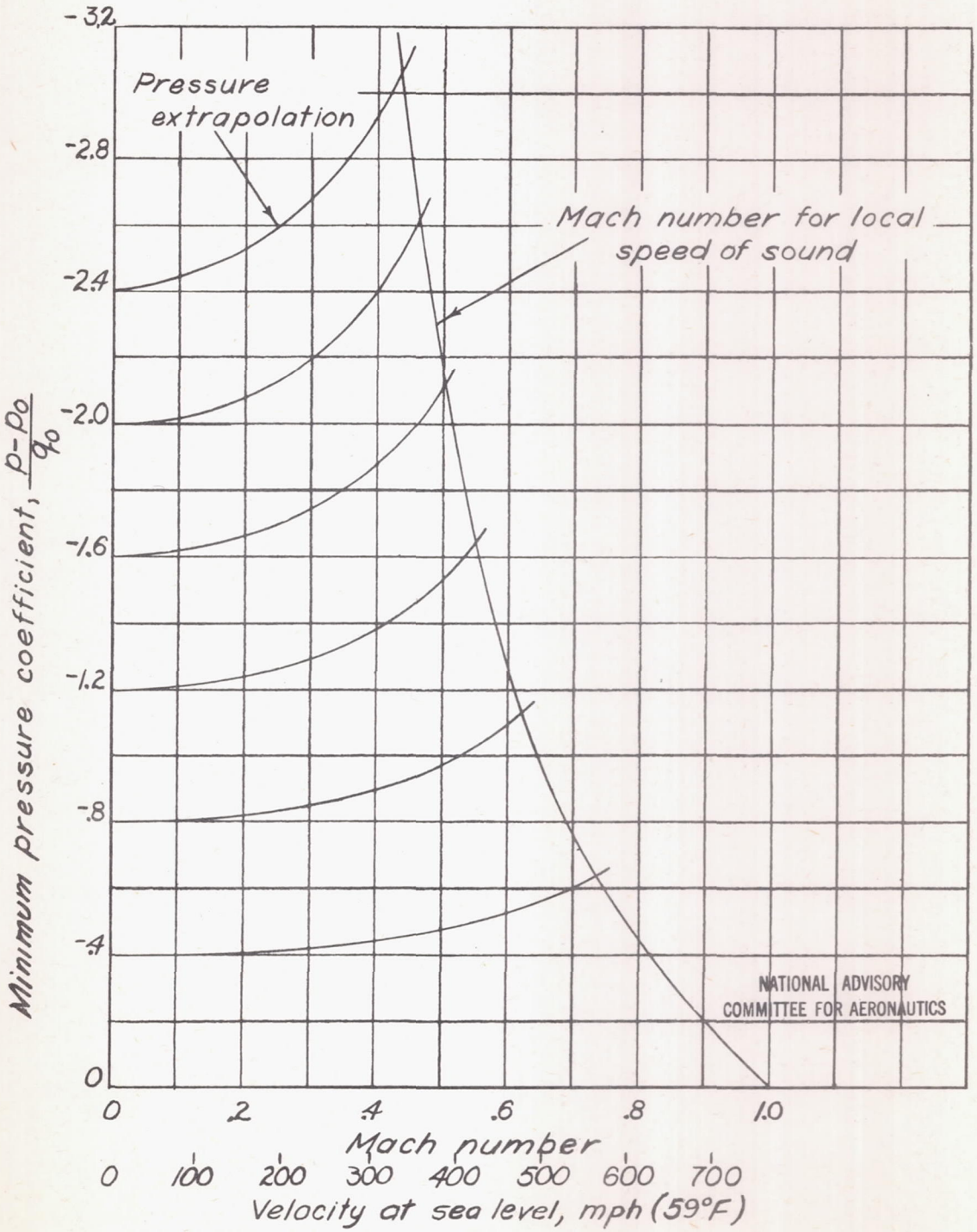

Figure 26. – Pressure coefficient against Mach number for determining critical speed. (See reference 5.)

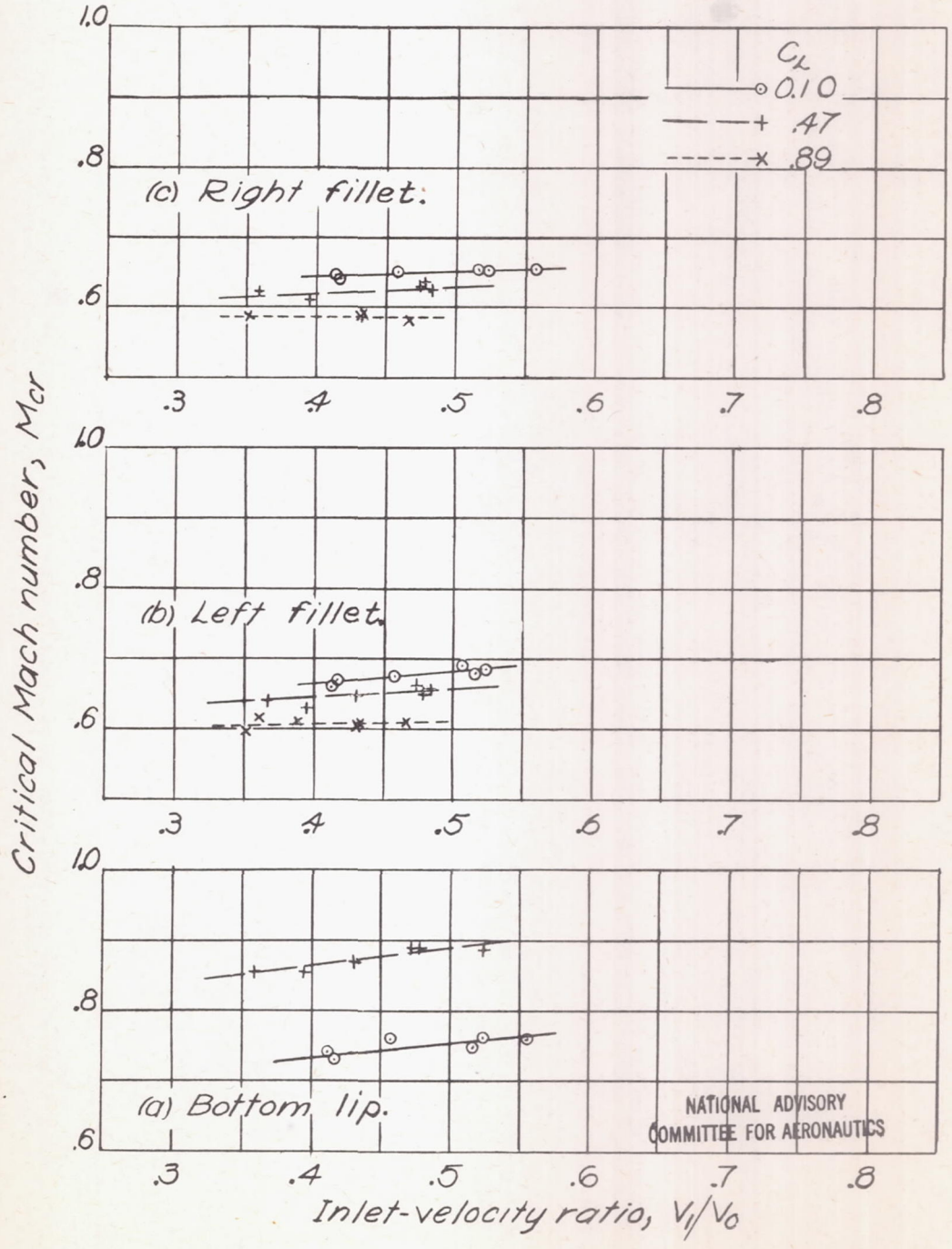

Figure 27. – Variation of critical Mach number with V_i/V_o. Small forward underslung duct; propeller removed.

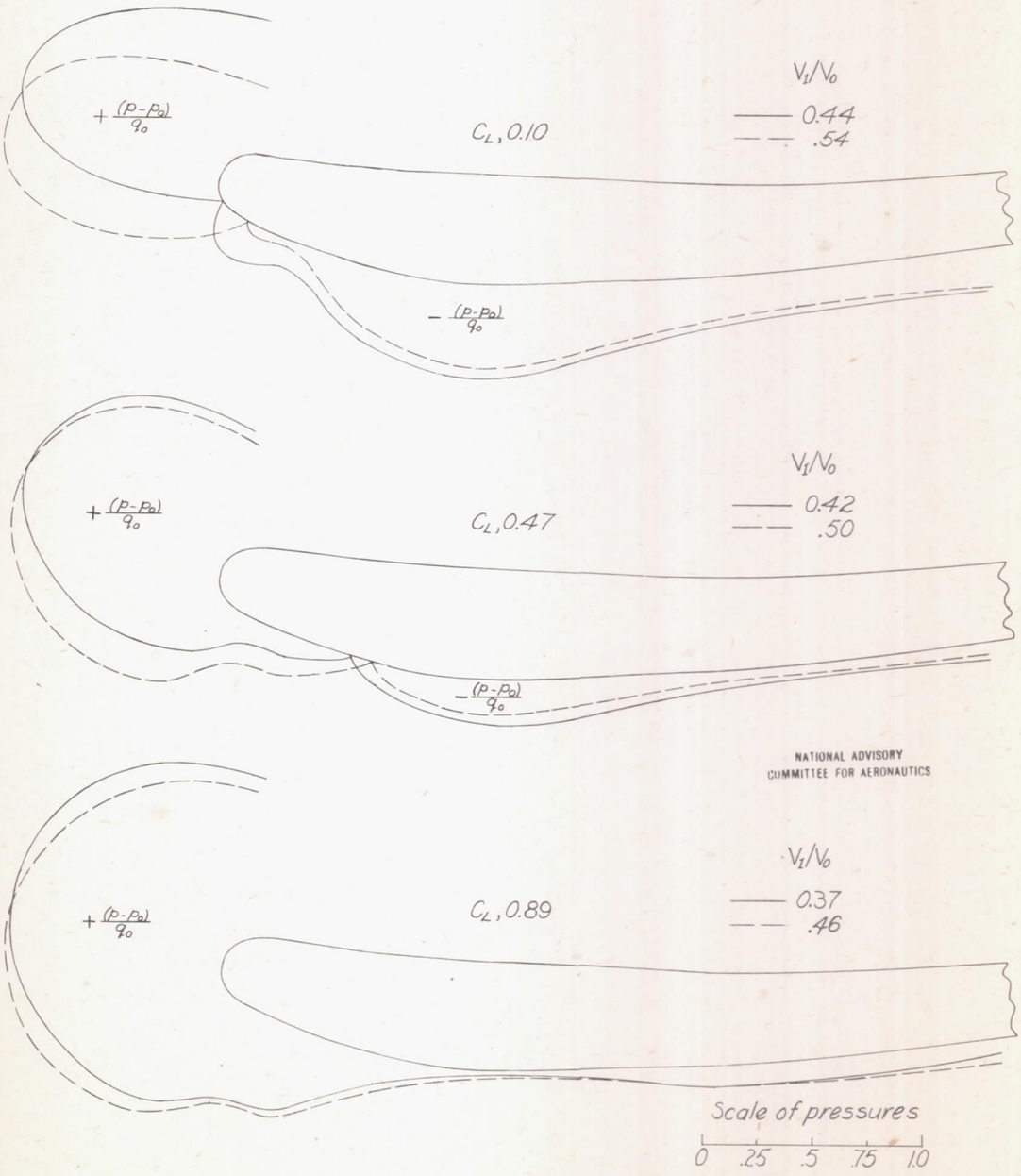

Figure 28.—Pressure distributions over bottom lip of the small forward underslung duct.

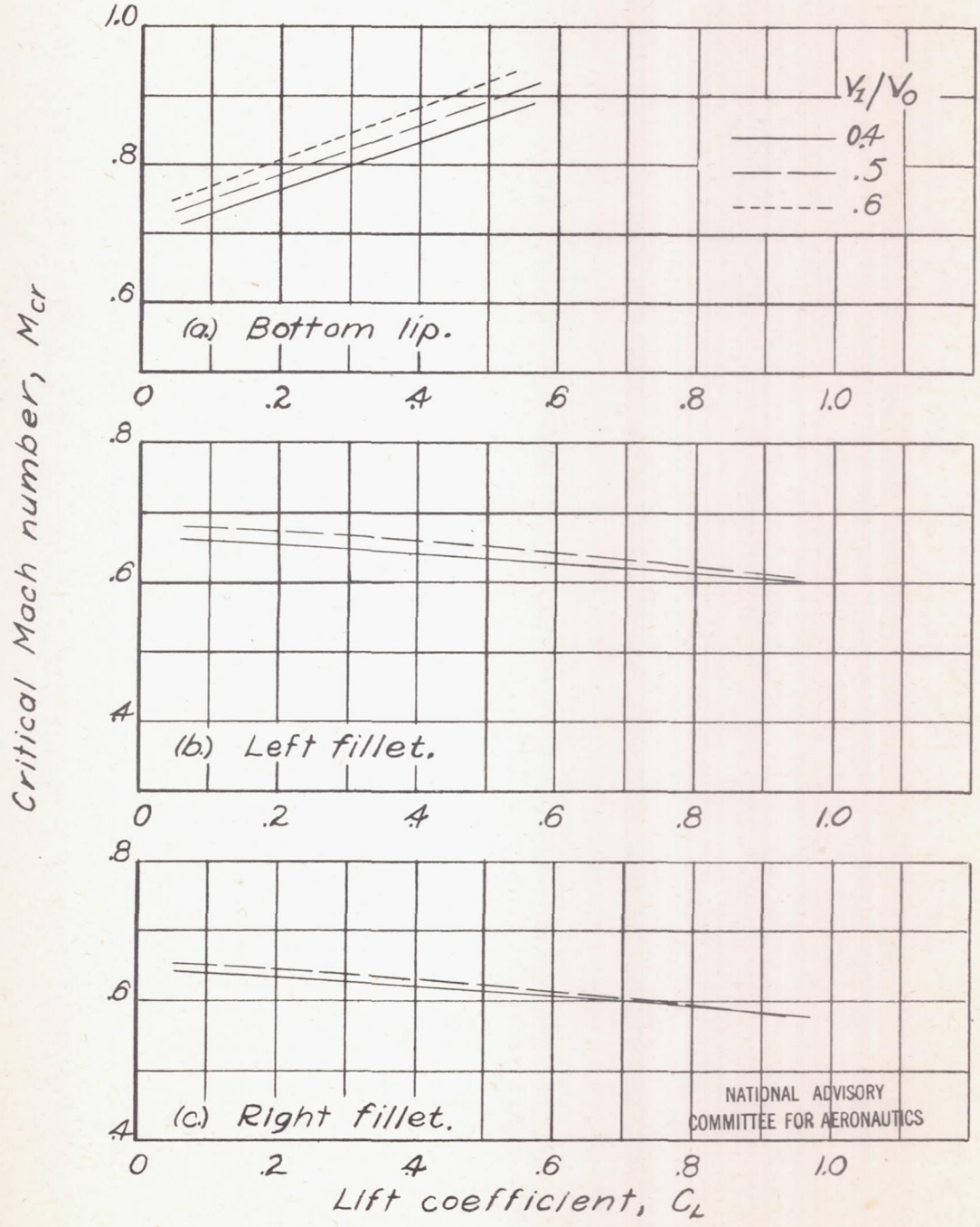

Figure 29. — Variation of critical Mach number with C_L. Small forward under-slung duct; propeller removed.

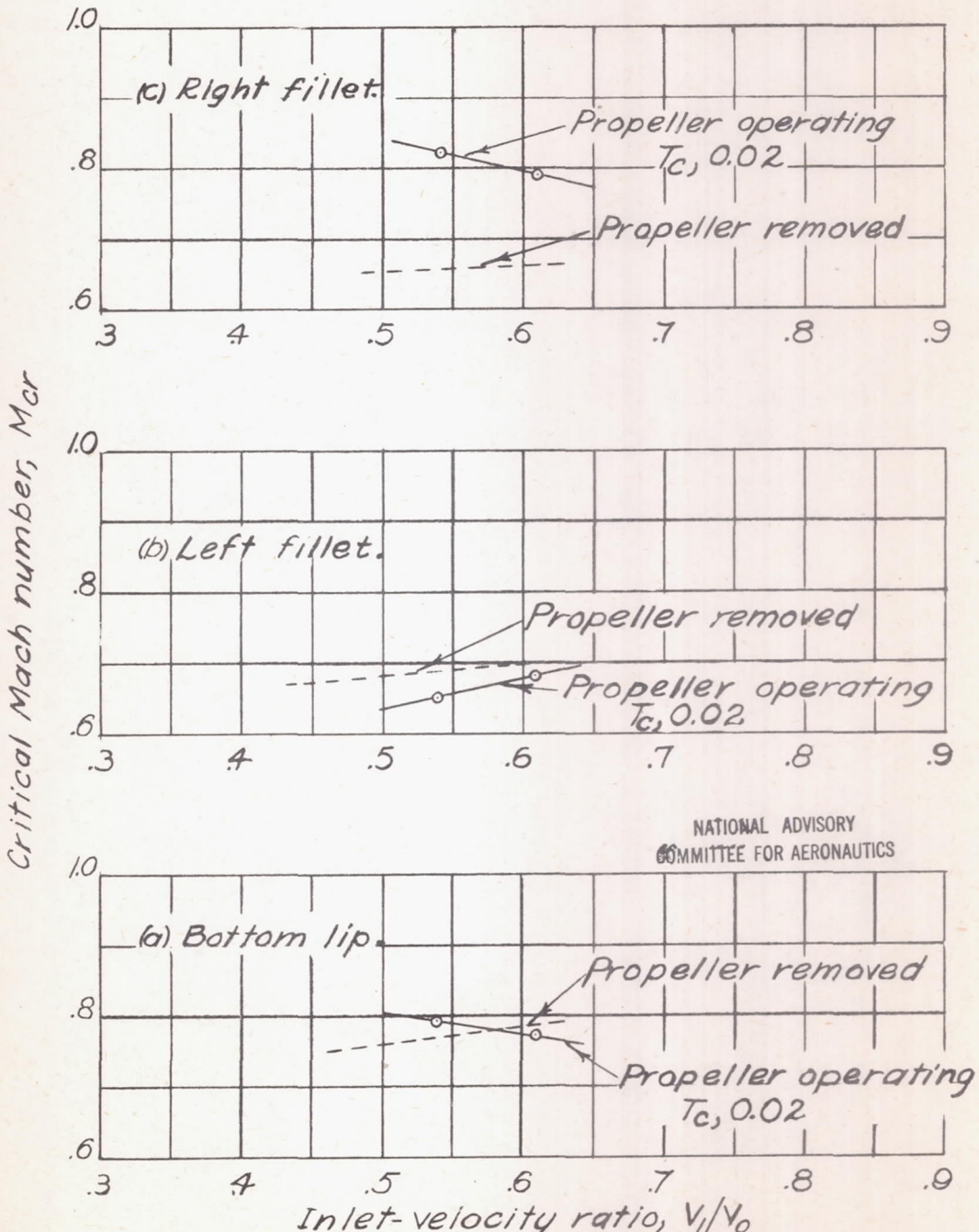

Figure 30. — Variation of critical Mach number with V_i/V_o. Small forward underslung duct; propeller removed and operating; C_L, 0.10.